Thesis for The Degree of Licentiate of Engineering

Enabling collection of data – from lab to field – to forecast battery ageing

Kasper Westman

Department of Physics
Chalmers University of Technology
Gothenburg, Sweden, 2024

Enabling collection of data – from lab to field – to forecast battery ageing

Kasper Westman

Department of Physics
Chalmers University of Technology
SE-412 96 Göteborg,
Sweden
Phone: +46(0)31 772 1000

Printed by Chalmers Digitaltryck,
Gothenburg, Sweden 2024.

"And I think I've found the real benefit of digital memory.
The point is not to prove you were right;
the point is to admit you were wrong."
- *Ted Chiang* The Truth of Fact, the Truth of Feeling

Abstract

By 2030, the battery industry is predicted to have an annual output of over 4 TWh of storage capacity, thus supporting the "electrify everything" paradigm. This comes with societal benefits such as lower CO_2-emissions in the end applications, but also with risks of over-consumption and too high life-cycle emissions. Thus, making sure that batteries last longer by mitigating degradation is paramount. Here we explore how mechanistic understanding of degradation can be gained and effectively communicated for use in a battery digital twin (BDT), in it's turn capable of predicting future battery degradation and suggest mitigating actions.

This is achieved by conducting a campaign of lab-based experiments to identify relevant degradation modes. Simultaneously a battery information format (BIF) suited for field application is developed within the scope of this thesis. The BIF is framed so as to respect both qualitative and quantitative needs existing in battery powered applications and those from a broader informatics perspective. The knowledge about degradation modes are successively encoded into a graphical causal model (GCM) that is consequently used to define the binning scheme of the BIF-compatible histograms, enabling a memory-efficient data-collection strategy.

The method is showcased for a Hard Carbon and $Na_3V_2(PO_4)_2F_3$ sodium-ion battery, utilizing 1 M $NaPF_6$ as electrolyte, and identifying degradation using electrochemical techniques (e.g. galvanostatic cycling and electrical impedance spectroscopy), coupled gas-chromatography/mass spectrometry, infrared spectroscopy, and EDX analysis. Subsequently the mentioned translation into a BIF-compatible data collection strategy is carried out. For next steps we suggest doing a field deployment of the strategy, either with the investigated chemistry or with commercial cells of a similar chemistry, so as to validate the BIF concept.

List of Publications

Appended publications

This thesis is based on the following publications:

I **K. Westman**, R. Dugas, P. Jankowski, W. Wieczorek, G. Gachot, M. Morcrette, E. Irisarri, A. Ponrouch, M. R. Palacín, J.-M. Tarascon, and P. Johansson,
Diglyme Based Electrolytes for Sodium-Ion Batteries
ACS Applied Energy Materials 1, 6, (2018), 2671–2680.

II **K. Westman**, A. Aitio, V. Nilsson, P. Johansson,
Perspective: The battery information format (BIF): A memory-efficient standard for communicating cell usage and operational capability for battery digital twins (BDTs)
Submitted, under review.

Other publications

The following publications were published during my PhD studies, or are currently in submission/under revision. However, they are not appended to this thesis, due to contents overlapping that of appended publications or contents not related to the thesis.

[**a**] P. Johansson, S. Alvi, P. Ghorbanzade, M Karlsmo, L. Loaiza, V. Thangavel, **K. Westman**, F. Årén,
Ten Ways to Fool the Masses When Presenting Battery Research.
Batteries & Supercaps 4, 12, (2021), ***1785-1788****.*

Acknowledgements

Conducting a Ph.D. project with the ground beneath one's feet in near-constant motion is something I would not recommend to anyone who appreciates sanity. The only reason it has still been possible for *me* is the dedicated support I've received from several patient and supportive people in my surroundings. First of all, Prof. Patrik Johansson has provided a fixed point of contagious *can-do* attitude alongside his excellent supervision that has made it possible to push through both intellectual and bureaucratic hurdles.

Similarly, I am immensely grateful for the (early) professional and scientific guidance provided by Björn Fridholm, Pavel Calderon, Viktor Nilsson, and Antti Aitio. For the latter, it can't go without saying that the decision by Antti, Tim Engstrom, and the rest of Elysia to take me on happened at a crucial time; where at first many things seemed lost, joining the team in UK turned out to be a bright silver lining. I can't wait to continue exploring problems in the battery space together and truly believe we have the potential of nudging the world in a better direction.

From 2020-2023, I want to thank the team at Nortical, especially the early technical founding team and our CEO Axel. Providing an environment where product development, start-up life, and academic research can coexist is not an easy thing, but you made it work. Thanking the team at Nortical without also mentioning our patrons would be negligent. Thus, to both the large investors, including Norrsken VC, Almi Invest, and E14 Invest, and to the smaller ones, including Christine Bjärkby, Mikael Gyllenhammar, and Adam Nilsson, I express a heartfelt thanks for making this possible in the first place.

Likewise, I want to acknowledge the financial support provided by the Kamprad Family Foundation within the Research and Innovation Program (Grant No. 20200165), the Swedish Research Council (Grant No. 2021-00613), and VINNOVA/Batteries Sweden (BASE) (Grant No. 2019-00064) for supporting the BIF project.

Yet another thanks I want to direct to all my former and present colleagues at MP division at Chalmers for all interesting corridor and lunchroom discussions. In particular, I want to praise Sajid for always providing an interesting perspective on life and for introducing me to the world of good coffee, and Patricia for being thrown into my project with short notice and quickly helping out with everything from detailed proof-reading to paperwork.

Finally, the most important people deserves their own section. Thank you Lisa, my partner, who has supported me in this endeavour and dream for almost half a decade. I know you often wish I had stayed on the beaten path and your willingness to let me stray is an act of love I will hardly forget. Also thank you Alvar—2.5 years old at the time of writing—for being a near-constant ray of sunshine, for showing me why I should do the things I do, and for challenging me in completely unexpected ways.

Table of Contents

Chapter 1

Introduction

Since the commercialisation of the lithium-ion battery (LIB) in the early 1990s, a slow but steady transformation has taken place in how we view and implement storage of electrical energy at a societal level. The transformation is mainly fueled by the realisation that climate change and environmental decline impose a significant risk for the future of human civilization and our standards of living. One of the most notable technology and consumer shifts relates to the transition from vehicles with internal combustion engines (ICEs) to electric vehicles (EVs) promising a tank-to-wheel energy conversion free from CO_2 emissions.

Within this "electrify everything" paradigm [1] many pitfalls still remain when one seeks true sustainability from both the environmental and social points of view [2]. In the environmental dimension the massive increase in LIB production carries a substantial energy and CO_2 footprint that in the short term could risk outweighing potential long-term benefits [3]. In the social dimension, sourcing of raw materials for LIBs risks affecting local communities adversely, the main focus having been put on workers conditions in cobalt mining in D.R. Congo, and to some extent lithium extraction in the Lithium Triangle in South America [4].

A cousin to the LIB, the sodium-ion battery (SIB), has recently entered a phase of pre-commercialisation and has the potential of addressing challenges related to material sourcing and scarcity but may not substantially improve the CO_2 footprint [5] when normalised for energy density. Thus, reducing over-consumption and minimising social and environmental footprints require us to make the most out of all SIBs and LIBs produced, maximising their utilisation, often synonymous with minimising their degradation.

1.1 Scope

This thesis outlines two strategies to understand and limit LIB and SIB degradation: (1) building mechanistic understanding of degradation phenomena to suggest interventions and (2) using the understanding to design field data that enable robust and actionable data-driven models to forecast degradation.

1.2 Lithium-ion and sodium-ion batteries

1.2.1 Galvanic cells

Galvanic cells are defined as devices able to store electrical energy as chemical energy. In daily life, we usually talk about "batteries" but strictly speaking a battery is a device comprising many galvanic cells. In the remainder of this thesis we will use the words "galvanic cell", "cell" and "battery" interchangeably, but for the latter we will indicate whenever a multi-cell system is considered by using the term "battery pack". In the standard LIB and SIB cell, two electrodes of different electrochemical potential are kept apart by a separator, preventing electrode contact and short circuiting (Figure 1.1). The electrodes are made up of an active material (AM), a conductive additive, such as carbon black, serving to improve electrical connection between AM particles, and a binder that keeps everything together (Figure 1.2) [6]. In conventional battery manufacturing, the electrode is coated as a slurry on top of a metal foil, serving to provide mechanical stability and an evenly distributed surface current [7].

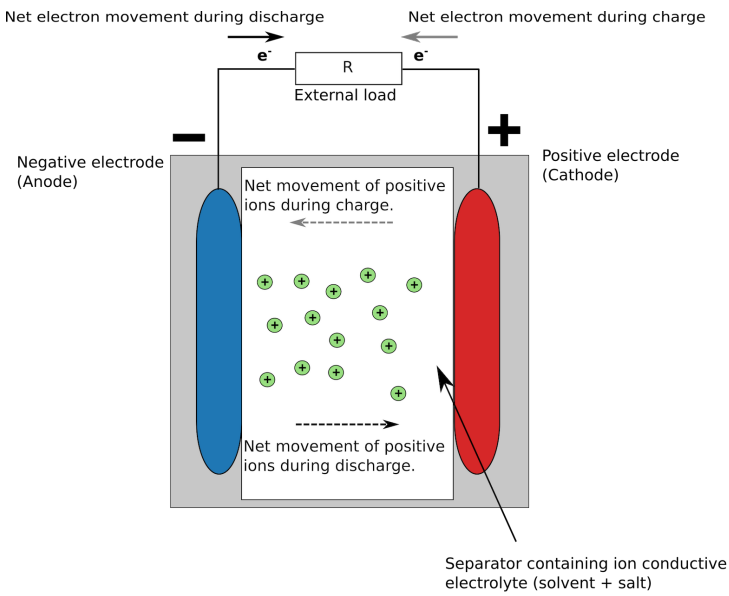

Figure 1.1: The fundamental principles of a galvanic cell.

To allow for ion transport between the electrodes, closing the inner circuit of the battery, the cell is filled with electrolyte, residing in the pores of the separator and those of the electrode composite structure. For the latter, the amount and size of pores can vary greatly with particle sizes and other process parameters. The electrolyte is electrically isolating to prevent cell self-discharge and mainly consists of a salt containing the ion of interest that is dissolved in an organic solvent [8]. Optimally the electrolyte should be oxidatively stable at the redox potentials of cathode and reductively stable at the redox potential

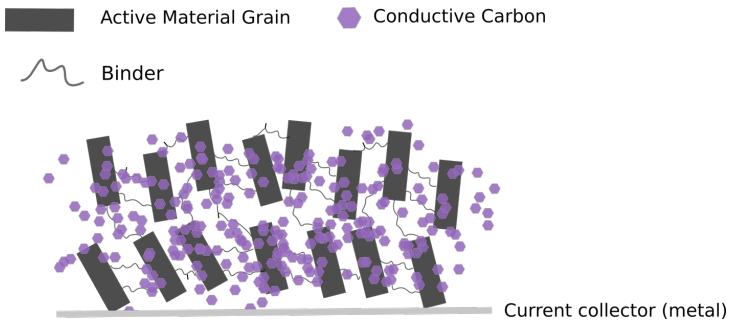

Figure 1.2: Conventional components of an electrode coated on a metal current collector.

of the anode to avoid causing unwanted side-reactions. This is also known as having a broad electrochemical stability window (ESW) [9].

When discharging a galvanic cell, the electrodes are connected by an external load. Because of a difference in redox potential associated with the anode and cathode, electrons will start flowing through the outer circuit [7]. At the same time ions will flow in the electrolyte to maintain global charge neutrality. The flow of electrons and ions is sustained by a continuous oxidation of anode species and a continuous reduction of cathode species, commonly known as a "faradaic current". In a battery, such a redox process gradually lowers the total internal energy of the system, the current being sustained until the full capacity of either of the active materials has been depleted. When charging a galvanic cell, the opposite process takes place: Energy is supplied to the system and stored by reversing the flow of ions and electrons, causing the internal energy of the system to increase. At any point in time the state of charge (SOC), denoted by the variable z, is determined by the fraction

$$z = \frac{Q_{avl}}{Q_{tot}}, \tag{1.1}$$

where Q_{avl}, the available discharge capacity, is the number of ions (M^+) that at any given time are available to move from the anode to the cathode, and Q_{tot} is the highest possible value that Q_{av} could attain, limited either by the total inventory of ions, or the sites available for intercalation in the cathode or anode [10].

The total discharge capacity, Q_{tot}, is dependent on the type and amount of active material used on both electrodes and on how the cell has degraded. The potential at which extraction or insertion of ions and electrons takes place will be dependent on the material structure and instantaneous composition. This makes the total percentage of inserted/extracted ionic charge carriers a factor determining the cell open circuit voltage, $V_{ocv}(z)$, i.e. the cell potential in the no-load condition, the "z" indicating the functional dependency on SOC.

Several factors determine the performance of a cell: first, we desire high gravimetric and volumetric **energy density**. To calculate the energy of the cell we integrate the cell voltage with respect to capacity, expressed as

$$E_{cell} = Q_{tot} \int_0^1 V_{ocv}(z)\, dz. \tag{1.2}$$

Second, high **reversibility** upon cycling is paramount, a "cycle" being defined as one complete charge and discharge within the allowed cell voltage limits. Irreversibility indicates how well discharge capacity is preserved both after the first (initial) and successive cycles. Initial irreversibility, $Q_{1,irr}$, is defined as

$$Q_{1,irr} = Q_1^c - Q_1^d, \tag{1.3}$$

where Q_1^c and Q_1^d denotes the charge and discharge capacity at the 1^{st} cycle, respectively. For any cycle, "n" we can furthermore define a coulombic efficiency, η_n^{ce}, communicating the fraction of discharge and charge capacity, i.e.

$$\eta_n^{ce} = \frac{Q_n^d}{Q_n^c}, \tag{1.4}$$

and thus also serving as a measure of how reversible each cycle is. For commercial LIBs, η_n^{ce} is usually above 99.991 % , ensuring that cell capacity reaches 80% of it's beginning-of-life (BOL) value after more than 3000 cycles [11] .

Third, we desire a low cell **polarization**. This is defined as the voltage drop observed under load and can be defined as a combination of the linear and non-linear effects of having current passing through the cell. Denoting the current by i, designating a positive current for charging, we can express the cell voltage and polarisation as

$$V_{cell}(z, i, T) = V_{ocv}(z) + \underbrace{iR_0(T) + f(i, z, T, \theta, t)}_{\text{Polarisation}}, \tag{1.5}$$

where $iR_0(T, z)$ denotes an ohmic effect, albeit with a temperature (T) and SOC dependency, and $f(i, T, z, t, \theta)$ gathers all non-linear effects that depend both on current, cell temperature, SOC, time, as well as internal states of the cell, θ, relating to ageing of materials. The non-linearities in the cell arise due to transport and double-layer effects within the cell. Polarisation, also referred to as voltage drop due to cell internal resistance, determines both the energy efficiency of the cell and, consequently, how much heat is generated when (dis)charging the cell, thus impacting the cells power capability.

Finally, cells must be **safe** to not risk damage to persons or property, even if the case where batteries are mishandled by users. A somewhat elusive state-of-safety has been proposed in literature to denote the instantaneous safety level of a battery as an inverse of the amount of abuse the cell has been subjected to according to

$$\text{SOS} = \frac{1}{f_{abuse}(\mathbf{x})}, \tag{1.6}$$

where f_{abuse} is an arbitrary abuse function that takes on values from 1 to $+\infty$ [12]. Another definition is to assume the SOS indicates the risk of a thermal event happening within a given time horizon, t, given the usage history (UH):

$$\mathrm{SOS}_t = 1 - p(\text{thermal event before t}|UH). \tag{1.7}$$

This is similar to what is proposed by Preger *et al.* [13].

1.2.2 The solid electrolyte interphase

Enabling safe LIBs and SIBs with low polarisation and a long cycling life does not only imply developing thermodynamically stable electrolytes and electrode materials in isolation. The interfaces between the electrolyte and the electrodes, emerging in the full cell, are just as important. Many commercial solvents used in LIBs and SIBs have appropriate oxidative stability but are reduced at the potentials reached at the anode, meaning that ionic charge carriers would continuously get lost were there no balancing mechanism. The solution to the problem comes from the kinetics of electrolyte decomposition [8]. As predicted by reduction potentials, there is an initial solvent decomposition. However, instead of continuing the reaction, the decomposition products create a film and passivate the surface. The film, commonly called the solid electrolyte interphase (SEI), is formed during the first charge and then stabilised during subsequent cycles [8]. Novák *et al.* have described properties of an ideal SEI, noting that it should be electrically insulating, leading to prevention of further electrolyte breakdown, but also a good ion-conductor, leaving kinetic performance and polarisation of the cell unaffected [14]. Another quality would be that they are insoluble in the solvent used for the electrolyte, leaving a stable film.

Understanding the morphology and structure of the SEI is thus motivated by a wish to deliberately tune it to give the longest cell cycle life and lowest polarisation. Complete understanding of the SEI remains a challenge that has been tackled in numerous ways. For example, G. Gachot *et al.* [15] studied SEI chemical composition using gas chromatography and mass spectrometry (GC/MS) coupled to Fourier transform infrared (FTIR) spectroscopy. Primary and secondary electrolyte decomposition products of $LiPF_6$ in cyclic and linear carbonates, such as EC-DMC (Figure 1.3) were identified using this method [15], [16]. For SIBs, the higher redox potential of Na limited the rate of further reduction of decomposition products, such as diethylene carbonate. The lack of reduction indicates that the SEI would have a different character and a different (worse) performance in terms of stability [17], [18].

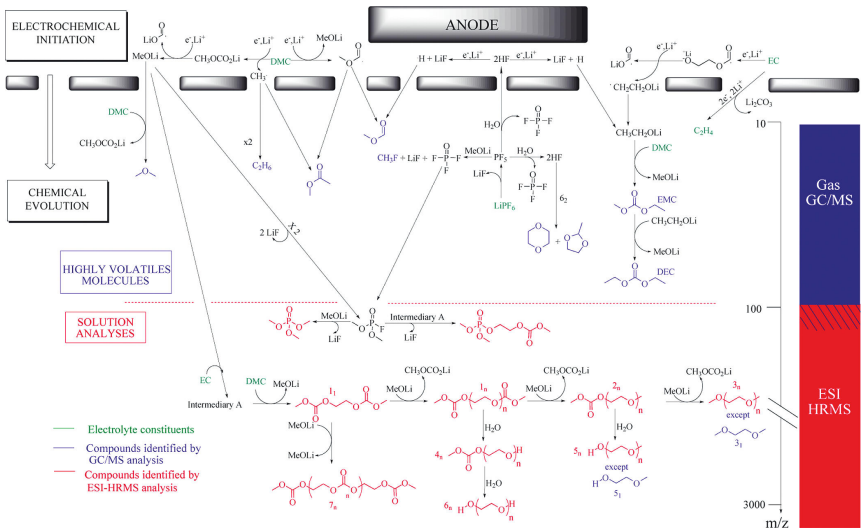

Figure 1.3: Decomposition scheme taking a range of different LIB processes into account when using carbonate electrolytes. Reprinted with permission from [15]. Copyright 2011 American Chemical Society.

Similarly, Seh *et al.* conducted a study on the glyme family of solvents [19], [20]. Employing X-ray photoelectron spectroscopy (XPS), the authors claimed to observe anodic ether reduction products of cycled surfaces. The reduction was proposed to yield a very thin layer of $ROCH_2{-}Na$ species on top of a layer of inorganic NaF and NaO_2 species. Furthermore, they demonstrated how a diglyme-based electrolyte leads to a very efficient plating-stripping behaviour which they attributed to the stability and mechanical properties of the aforementioned film [19].

1.3 Battery degradation

From an engineering perspective, cells reach their end-of-function (EOF) when they can no longer provide useful energy and/or power (Figure 1.4). The useful energy and power can be expressed by cell capacity and resistance/impedance, respectively: low capacity and high resistance diminishes useful energy, while power is mainly limited by high resistance.

Often in literature and industrial settings, however, it is only the estimated Q_{tot} divided by the nominal, BOL capacity of a cell that is used to express a state-of-health (SOH) metric. Such aggregation risks masking the fitness of a cell to perform any specific function, when other factors such as energy efficiency and self heating rates are also important to understand. EOF can also be reached when the SOS is deemed too low. Even though manufacturing defects are among the most detrimental factors for SOS [21], [22], a rough correlation also exists to resistance growth and capacity fade [23].

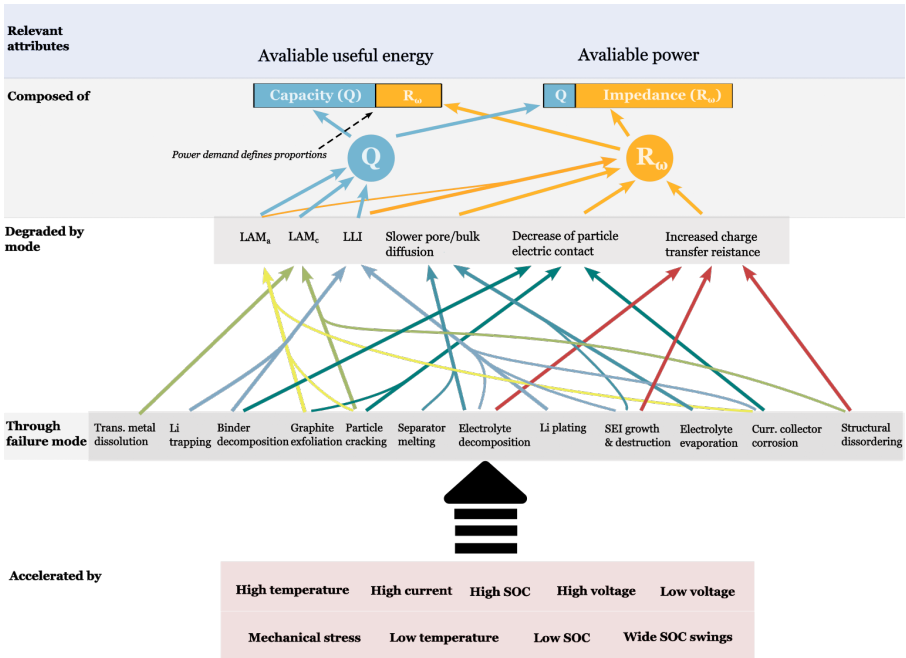

Figure 1.4: The connection between usage conditions and their impact on failure modes, degradation modes, and subsequently on battery performance metrics.

Below we present a causal tree of degradation, and identify "stressors" [24] as the operating condition(s) inducing a specific failure mode, successively leading to observable degradation modes and, finally, to changes in capacity and internal resistance. The focus is on LIBs and SIBs, but many of the main mechanisms illustrated, e.g. SEI-growth or particle cracking, are likely to be valid for the many next generation battery technologies, such as solid-state (lithium) batteries [25], Ca metal [26], lithium-sulfur batteries [27], etc.

Stepping through some specific parts of the hierarchy of Figure 1.4, loss of cell capacity (Q) can be divided into loss of (anode/cathode) active material ($LAM_{a/c}$) and loss of lithium inventory (LLI) [28]. For LAM, the mechanism involves sites for lithium insertion being lost due to structural changes at the micro or meso-scale, such as cracking upon cycling due to volume change [29], AM particles disconnecting from the electrode, or resistive surface film formation [30]–[34]. Cracking can be worsened by rapid (local) insertion, meaning that both wide swings in average electrode lithiation, i.e. SOC, and high, sustained, current can cause LAM. Local insertion errors are promoted by current density heterogeneities, which develop more easily in thick electrodes with high mass loadings, and low temperatures. LAM_c may happen due to irreversible phase transitions or structural disordering of the AMs, most often at low levels of lithiation, as in NMC811 at high cell voltages and high SOC [35]–[39]. It can also be caused by transition metal dissolution into the electrolyte as for LMO

cathodes at high temperatures and SOC [40].

LLI on the other hand is caused by parasitic reactions, mainly due to the formation of the solid electrolyte interphase (SEI) at the anode surface, and AM sites becoming electrically isolated within the electrode [41]. The SEI forms and consumes cyclable ions primarily during the first cycle(s), also known as "formation cycles", but continues to develop during operation, stimulated by low anode potentials, globally corresponding to high SOC/high cell voltage, and locally promoted by high sustained charging current and rough particle morphology [42], [43]. Higher temperatures will further promote SEI (re)growth by speeding up kinetics, while also causing the existing SEI to dissolve, exposing new surfaces for the electrolyte to decompose at.

Furthermore, there are negative synergies; LLI is partly triggered by LAM_a as when electrode particles crack, fresh surfaces are exposed for electrolyte decomposition and SEI growth. This is of particular concern to SIBs, where the solubility of SEI components in the electrolyte is higher than for LIBs, further increasing the temperature sensitivity of degradation [44]–[46]. LLI can further occur due to metal plating. Apart from the loss of cyclable ions, this can cause dendrite-growth, tree-like structures that eventually risks short-circuiting the cell. Metal plating occurs at low anode potentials and is hence promoted by high SOC/cell voltages and also by high sustained charging current at low temperatures.

Cell internal resistance (R_ω) increases partly due to the same reasons as capacity loss; meso/microstructure evolution decreases the electronic contact and conductivity within the electrode, while the growth of the SEI makes ion transport slower, both by limiting access to single particles and by decreasing ion mobility/diffusivity within the porous electrode. Electrolyte loss, accelerated by high temperature, poor cell design, and SEI formation, will further increase the internal resistance. R_ω is dependent on the observation timescale/frequency, hence the ω subscript, and observably higher at long timescales, due to a richer set of mechanisms contributing to the voltage response of the cell, which also means that the R_ω timescale dependence may change as the cell ages (also refer to the part on polarisation in Section 1.2.1).

For SOS we consider the risk of catastrophic failure, which for a cell mainly happen due to exothermal decomposition reactions. Since LIB electrolytes contain highly flammable solvents a fire is easily sustained once started [47], [48]. Rapid SOS decline can often be traced back to cell manufacturing defects, as in a major OEM vehicle recall in 2021 [21], [22]. A SOS decline can be caused by dendrite growth, gas formation, as well as ageing-induced inhomogeneity of electrode resistance, leading to local spikes in current density, thus inducing material decomposition, especially if the battery management system (BMS) is not ageing aware [21], [48]. SOS can in fact also improve upon usage due to a decrease in the energy stored [13]. Preger et al. showed that the empirically most well-supported SOS decline hypothesis is that cycling below 25°C increases the risk of thermal runaway, but also that this can often be mitigated by allowing a cell to rest [13]. Overall, SOS is highly dependent on the ageing trajectory.

1.4 Connected battery packs and digital twins

From an application perspective, it is often the battery pack that serves as the relevant design unit. Here we give a general outline of the topology of a battery pack, urging that there is a high variability between manufacturers and applications. Battery packs are often composed of several modules (Figure 1.5, grey boxes), serving as conveniently sized mechanical units and logical units communicating with the BMS on an pack-internal communication bus [49].

The BMS is an embedded computer responsible for functions such as receiving and processing sensor data, ensuring safe operation of the battery pack, estimating cell SOC/SOH, logging important information, and communicating with the rest of the application (Figure 1.5, red lines) and the outside world, e.g. via a telematics module. The pack can further be fitted with a system that provides active cooling (or heating) to the module or the cells in the module. Often coolant flow and inlet/outlet temperature are measured (Figure 1.5, green F and green Ts, respectively). On the pack level, the pack voltage and current are measured (Figure 1.5, green "A" and "V" circles).

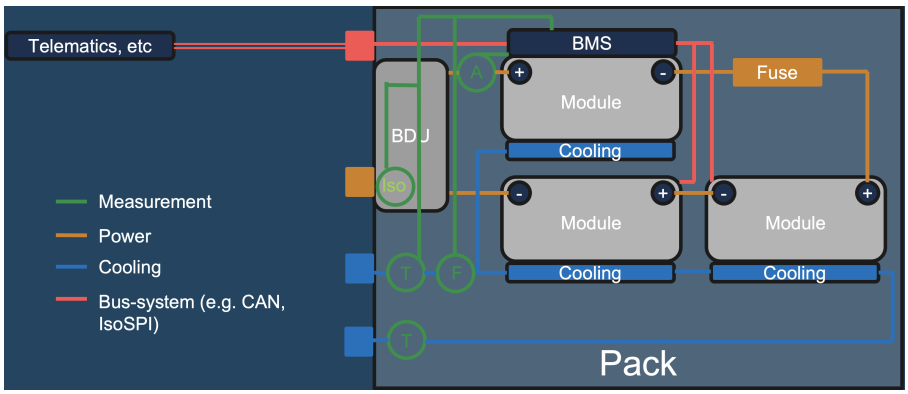

Figure 1.5: Common logical layout of a battery pack featuring several modules.

Stepping into the module level, these are comprised of several "supercells", each containing a number of physical cells connected in parallel (Figure 1.6, right). Across each supercell voltage is measured (Figure 1.6, left, green circles with "V"'s), either directly by the BMS or via an analog frontend chip (denoted "CVTN" in Figure 1.6, left) [49]. Also, temperature will be measured at several positions (Figure 1.6, left , green circles with T's), not necessarily coinciding with the number of cells due to the cost, complexity, and increased risk of single sensor failure associated with adding many temperature sensors [49]. Since configurations with supercells and modules in series are often preferred to increase pack voltage, it is in these cases sufficient to measured pack current (1.5, green I), since this will also be the current of each supercell (due to Kirchhoff's current law).

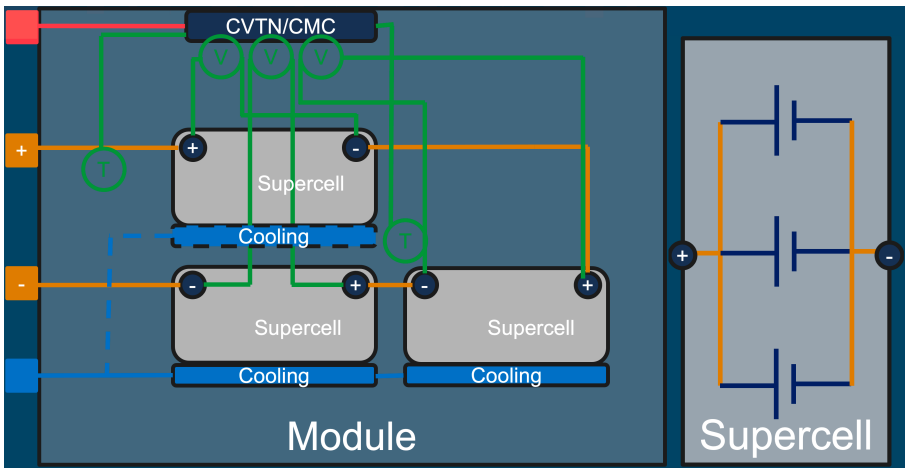

Figure 1.6: Logical layout of a module (left) composed of several supercells (right).

Information gathered within the battery pack from the sensor outlined above can be leveraged to establish a battery digital twin (BDT), consisting of three parts: i) a virtual model of the battery pack and its constituent cells, ii) a record of relevant meta- and usage data delivered by the battery, and iii) an information link between the physical battery and the data record, e.g. a telematic capability between the battery and a central storage [50]–[52].One such BDT concept is illustrated in the upper part of Figure 1.7. Here the capabilities of off-board computing and aggregation of data across several members of a fleet are used to train accurate prognostic models of battery health and remaining useful life (RUL). Furthermore, the BDT is used to propose optimal usage strategies for the battery pack, translated into control parameters that can be fed back to the real-world asset [52].

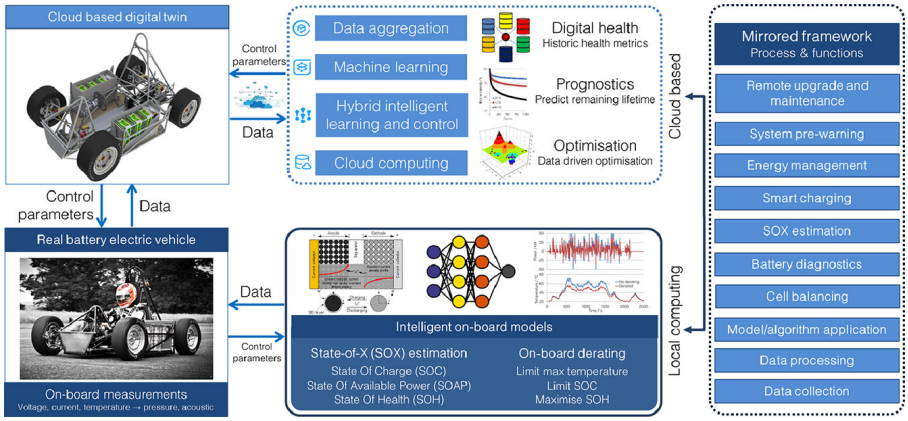

Figure 1.7: A BDT as proposed by Wu *et al.* [52].

Thus, a properly implemented BDT, closely coupled to a battery information format (BIF), standardising the inputs (a.k.a. *features*) and outputs (a.k.a. *targets*) of the BDT degradation models, can provide control of the battery degradation [52]–[55]. Ultimately it can also create a more reliable 2$^{\text{nd}}$ life and refurbishing market of batteries. This happens by virtue of lowering the uncertainty in forecasts of remaining battery lifetime, health, and safety. Accurate prognoses of battery capacity and electrical resistance allow for the trading of 2$^{\text{nd}}$ life batteries and battery cells at a higher price, by lowering information barriers and risk for the buyer, without having to conduct expensive end-of-(first)-life testing [56], [57].

Chapter 2

Methods, approach and experimental

In this chapter we outline both the theoretical background and the application of methods used in this project. The first part concerns lab-based measurements of degradation mechanisms carried out in Paper I, while the second part focuses on the theory and approach taken when designing a BIF (Paper II). The third and final section introduces the concept of causal graphical models, later used to combine results from the two papers.

2.1 Pinpointing degradation phenomena in the lab

In the experimental part of this work (Paper I) we studied a SIB system with diglyme as the electrolyte solvent. A number of techniques were employed to understand the full and half cell cycling stability, and to uncover what degradation mechanisms occurred, focusing mainly on the electrolyte. Below we outline the theory and application of the main methods used.

2.1.1 Experimental cells

The cells used in this project employed either Na-metal or Hard Carbon (HC) as an anode [58], [59], HC or $Na_3V_2(PO_4)_2F_3$ (NVPF) [60], [61] as a cathode and an electrolyte consisting of 1 M $NaPF_6$ [17] in diglyme (Figure 2.1) [20].

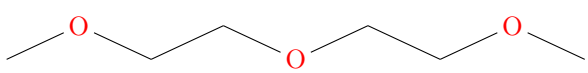

Figure 2.1: A diglyme molecule, used as electrolyte solvent in this project.

In the remainder of this thesis we express the cell setup according to the format

Anode|Electrolyte|Cathode,

sometimes omitting the electrolyte (and then only using one "|" symbol). The reason for using a HC|1 M $NaPF_6$ in diglyme|NVPF was the recent pre-commercialisation of HC|NVPF cells and initial studies showing great performance of diglyme for Na stripping and plating and appearing stable in SIBs [19] as compared to their LIB counterparts [62].

Dealing with mechanistic understanding of cells employing a new electrolyte we used experimental cells to reduce cost and be able to do easy disassembly and post-mortem of cells after experiments were run. Swagelock cells made out of stainless steel and coin cells were thus assembled according to Figure 2.2, left and right, respectively. Assembly was done in an argon-filled glovebox with the surrounding oxygen and water content being less than 10 ppm. The atmosphere was controlled in order to not contaminate the electrolyte with water, $NaPF_6$ being known to decompose and form corrosive HF in the presence of water, and oxygen reacting with Na metal to form impurities.

Within the cells, electrodes were placed on both sides of a boro-silicate glass-fiber separator. Electrode size was in the case of full cells controlled so that the balance was NVPF:HC 1.0:1.1. Furthermore, for coin-cells, a piece of Al-foil was cut and placed to completely cover the the cathode part of the casing to avoid corrosion of the stainless steel, shown to occur in previous tests. After putting the electrodes and foil in place, 120 µL of electrolyte were added to the separator using a pipette to ensure proper soaking.

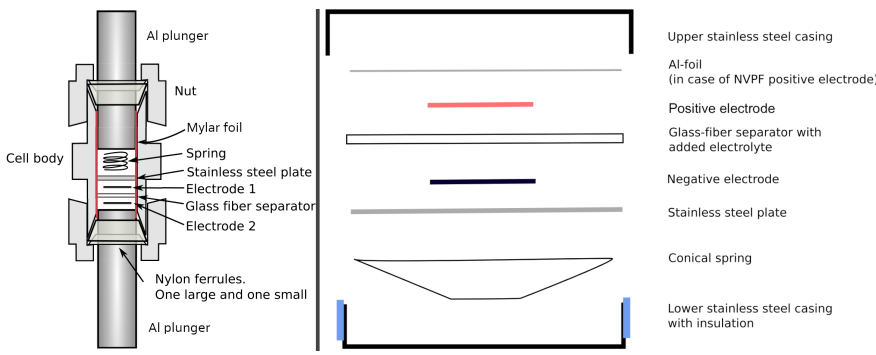

Figure 2.2: Schematic of Swagelock (left) and coin cell (right) assemblies.

For Swagelock cells (Figure 2.2, left), plungers were polished with a grade 1000 sandpaper to remove solid surface contaminants. The components were further cleaned and sonicated in ethanol and then in acetone and dried in a oven at 100 °C for 24 h to avoid water contamination. A Mylar® foil was used and cut to precisely cover the inner part of the cell body (Figure 2.2, left, thin red lines) to avoid corrosion of the cell. Mylar was used because of earlier experiments indicating that PTFE was degraded upon cycling in Swagelock cells employing Na-electrodes.

2.1.2 Galvanostatic cycling with potential limitation-GCPL

A common method to test electrode materials and cell setups is through galvanostatic cycling. By connecting the cells to a potentiostat that can track and regulate the current and voltage applied to the cell very precisely, arbitrary working conditions for a cell can be simulated.

Experiments are often run in either two or three electrode setups. In the latter case, two of the electrode potentials–denoted the counter- and working electrode–are constantly referenced against a third, reference electrode (Figure 2.3). With such a setup, the electrochemical processes taking place at the anode and cathode in a battery setup can be monitored independently. In a two electrode setup, one of the electrodes will instead serve as both reference and counter electrode. In this case, the proper working electrode potential can only be controlled if the electrochemical potential is constant at the counter/reference electrode, which is often (but not always!) the case when using alkali metal counter electrodes.

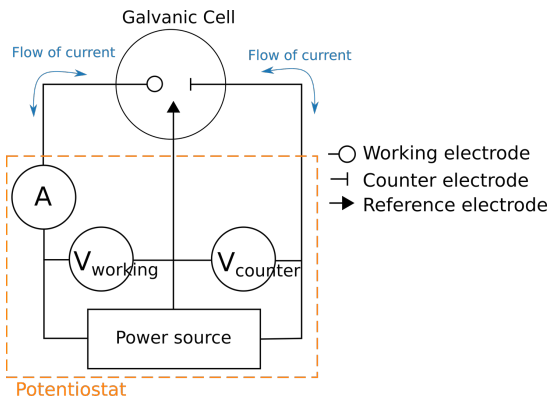

Figure 2.3: Principle of a three electrode setup. A current is measured between the counter and working electrodes. Voltages are measured with respect to a third, reference, electrode. Image adopted with permission from [63].

In galvanostatic cycling, the current is set to a constant value by the user. Mostly, a potential limit is also set for both charge and discharge of the cell. The setup tested can then be cycled between the upper and lower voltage cut-off limit for any number of times at the programmed current, while the total charge throughput during charging and discharging is tracked along with the voltage.

It is common practice to normalise the amount of current drawn in terms of C-rates, expressing the number of times the theoretical capacity of the active material is passed in one hour. For example, a rate of C/10 equals a current that will extract/insert the complete theoretical capacity from the electrode material in 10 hours. Since the C rate is dependent on the total amount of theoretical charge available, the current drawn during an experiment will vary with both the type and amount of active material used.

2.1.3 Cyclic and linear sweep voltammetry to track electrolyte stability

Conversely to galvanostatic cycling, cyclic voltammetry (CV) methods control voltage and current is the response variable. When interpreting cyclic voltammetry data, the current, I, detected at each voltage, V, is plotted in a so called voltammogram. Each peak in the voltammogram will correspond to a specific electrochemical process taking place [8]. A similar method, linear sweep voltametry (LSV), is used when it is relevant to scan a potential range only once at a fixed V/s rate. This is often employed when probing irreversible electrochemical breakdown of components.

In order to investigate degradation pathways relating to electrolyte decomposition, both oxidative and reductive stability was tested for 1M $NaPF_6$ in diglyme, using LSV. The oxidative potential limit was studied in Na half-cells using working electrode of NVPF, and mirror-like Glassy Carbon, and mirror-like foils of Al, Cu, and, Au. The cell voltage was then swept from 3 to 5 V vs Na^+/Na° at a rate of 0.1 mV/s, slow enough to clearly identify any electrochemical processes taking place. The onset potential for a process was defined to occur when the current density of the cell reached 50 $\mu A/cm^2$, the area of the electrode being 0.95 cm^2. Such a condition was consistent with previous work on electrocatalysis [64].

Reductive stability was similarly studied in half cells using working electrodes made of mirror-like stainless steel, glassy carbon,and foils of Al, Cu, and Au. These cells were cycled to 0V vs Na^+/Na° and any reductive peaks were recorded in the voltammogram. The wide selection of electrodes was used to rule out any contribution of activation energy impairing observability of the reduction process, assuming that at least one electrode would serve as a good catalyst for any potential parasitic reduction process.

2.1.4 Probing film growth on Na using electrical impedance spectroscopy (EIS)

The different mechanisms and regions that are present in any electrochemical system can be modelled as an equivalent circuit featuring a set of resistive and capacitive elements. As with every equivalent circuit featuring a network of passive components, it can be reduced to a single, frequency dependent, equivalent impedance. For example, the multilayered structure of the SEI will contribute with a certain phase shift and gain of any time dependent electrical signal. So will the transfer of ions in the bulk of the electrolyte and the transfer of electron in the bulk of the electrode [65].

By applying a small amplitude sinusoidal voltage at varying frequencies and tracking the current response, the equivalent impedance of a system can be probed and visualised in a Nyqvist plot. The reason for keeping the amplitude of the signal small is the nonlinear nature of transport and cell polarisation. Thus, making sure to control both the magnitude of applied voltage signal, and the temperature of the cell is crucial to guide interpretation of results. From the shape of the Nyqvist curve, it is possible to gain information about

system kinetics and transport properties [66]. Thus, it is also possible to detect any change or degradation taking place in the SEI structure or bulk of the electrode, as this would change the EIS spectrum over time [67].

To judge whether electrolyte decomposition resulted in a growing resistive SEI on the Na, an EIS spectrum was recorded in a Na|1 M $NaPF_6$ in diglyme|Na Swagelock cell at 25 °C. The measurement was done directly after assembly and then repeated every 6 hours for 96 hours. To stay in the linear impedance domain, we applied a 10 mV sinusoidal voltage, while frequencies were selected to capture a broad range, ranging from 0.02 Hz to 200 kHz with 10 points sampled per frequency decade. In each 6-hour interval the cell was left at OCV to let the growth of any SEI continue.

2.1.5 FTIR-spectroscopy of cycled cells

Fourier transform infrared (FTIR) spectroscopy involves illuminating a sample with broadband infrared radiation and recording reflected or scattered light. Because some frequencies of the incoming IR-radiation will match vibrational transitions in the sample, the response will be a modulated signal containing information about the frequencies that were absorbed. Illuminating a sample at an angle and taking advantage of the IR radiation being heavily absorbed in the bulk of the material sample studied, the technique can be used to probe surface layers chemical composition. SEIs from cycled surfaces in batteries could thus be analysed if they remain intact [68].

To determine if there was any SEI film formation on the surface of cycled hard carbon anode, FTIR was used to study 2 HC anodes cycled 2 times in full cells. The reason for not examining electrodes cycled more times was that any film formation is expected to happen mainly at the first and second cycles, since these cycles were associated with the largest irreversibilities. Cycled coin cells were disassembled under argon glove-box conditions and the HC anodes allowed to dry in the glove-box atmosphere for more than 24 hours. They were then transported in sealed coffee-bags to a nitrogen-filled glove-box equipped with an IR spectrometer. The cycled anodes were mounted in a praying mantis diffuse reflectance accessory (HARRICK) to allow for airtight transfer to the spectrometer. IR measurements were carried out in diffuse reflectance mode. To remove any contributions from the bulk hard carbon, a background of a pristine HC electrode was initially recorded. Also a spectrum was recorded for a HC electrode that had been soaked in the diglyme 1 M $NaPF_6$ electrolyte for 20 minutes and then allowed to dry for 2 hours in glove-box conditions. The soaked and dried electrode was made as a comparison, to record any effects arising solely from the electrolyte penetrating the electrode or evaporating, leaving a crystalline surface film behind.

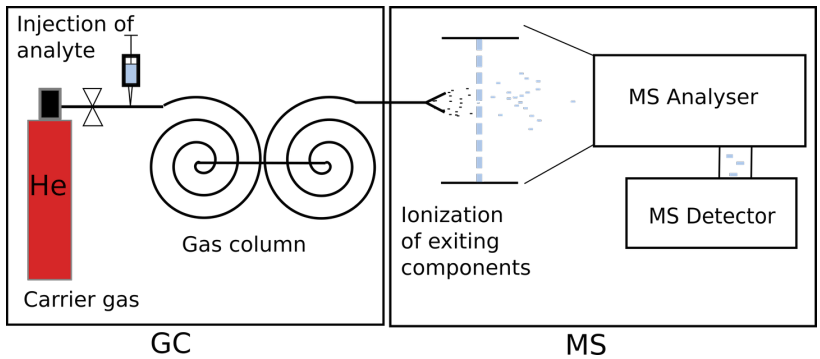

Figure 2.4: Principle of a GC/MS setup.

2.1.6 GC/MS to track electrolyte breakdown

The principle of coupled gas chromatography/mass spectrometry (GC/MS) setup is illustrated in Figure 2.4. For the gas chromatography (GC) part, an analyte in gas phase is injected into the column where a steady stream of inert gas is flowing. The gas flow then separates the different components of the analyte based on their tendency to be retained inside the column. Retention will in turn depend on the amount of interaction the component experiences with the column walls, which are often coated with a polymer to improve separation. In case the analyte was a liquid, it would first have to be heated for evaporation, thus limiting the detection to that of substances able to evaporate.

After the GC-column, the components separated will reach a mass spectrometer (MS) at different times. The mass spectrometer works by first ionising the analyte component and then separating the resulting fragments by their mass/charge ratio in the analyser. Each substance emerging from the gas column produces a cascade of ionised fragments serving as a fingerprint for the substance. In this way the contents of the analyte can be determined one-by-one [69], [70].

Complementary to the surface analysis offered by FTIR, liquid injection-GC/MS was employed to understand any decomposition products formed from the 1 M $NaPF_6$ in diglyme electrolyte. Results were then coupled to reduction schemes of the electrolyte. The separators from full cells that had been cycled 50 times and half-cells that had been cycled 10 times were recovered and soaked in 1 mL of dry acetonitrile to dissolve any degradation compounds. The separators were then removed from the soaking liquid and discarded. The remaining blend of acetonitrile and soluble compounds from the separator was diluted 100 times before being injected into the GS/MS setup, consisting of a trace 1300 series GC ultra-gas chromatograph coupled to an ISQ mass spectrometer.

Since this method would not allow for the detection of gases, another experiment was carried out where the electrolyte was stored together with Na metal for 48 days. Using the same setup as a above for gas gas-phase GC/MS, flushing the column and storage vessel with argon.

2.1.7 Half and full cell capacity tests

To study the interaction between actual electrode materials and the 1M $NaPF_6$ in diglyme electrolyte, half-cell galvanostatic cycling was performed in coin cells using Na-metal as an anode. The cells were cycled 15 times using the cut-off potentials given in Table 2.1.

Working electrode	Lower cut-off potential (V vs Na^+/Na°)	Upper cut-off potential (V vs Na^+/Na°)
HC	0	2
NVPF	2	4.3

Table 2.1: Cut-off voltages for cycling of materials in half-cells, using Na metal as counter electrode

Full cells of HC/NVPF where also cycled in coin cell, employing the cut-off scheme in Table 2.2. In the full cells, the electrodes were not completely balanced in capacity because of difficulties doing so with tape cast electrodes. Instead, the capacity ratio between carbon and NVPF was approximately NVPF:HC 1.0:1.1 based on charge capacity of the first charge in half-cells. Since HC capacity was in excess, the mass of active NVPF was used to set the C-rate.

Electrode setup	Lower cut-off potential (V_{cell})	Upper cut-off potential (V_{cell})
NVPF/HC	2	4.3

Table 2.2: Cut-off voltages for cycling of materials in full cells

2.1.8 SEM and EDX analysis of cycled anodes

Further complementing the FTIR and GS/MS analysis to study degradation in and on the HC anode of cycled full cells, scanning electron microscopy (SEM) micrographs of the anode were recorded. Before imaging, HC anodes from full cells had been cycled 1.5, 2 and 50 times in 1 M $NaPF_6$ diglyme electrolyte using the same cut-off voltages as in Section 2.1.7. Because of limitations in the movement of the stage of the microscope, the samples had to be transferred in air before being mounted inside the microscope.

Electrode setup	Lower V_{cutoff} [V]	Upper V_{cutoff} [V]	Cycles	Comment
Na|NVPF	3.5	4.3	1	
Na|HC	0	1.4	1	
HC|NVPF	2	4.3	10	Using materials from previous 2 rows after washing the NVPF.

Table 2.3: Cycling scheme for further exploring possible vanadium extraction.

Apart from imaging, Energy-dispersive X-ray spectroscopy (EDX) analysis was carried out on the samples to identify any elemental contamination. After detecting vanadium in the EDX spectra it was decided to investigate if the metal came from soluble species forming at the cathode and if it was only deposited during the first cycle. This was done by cycling a NVPF cathode in half cell and HC anode in half cell according to the scheme in Table 2.3. The half cells were then disassembled and the electrodes recovered. The NVPF cathode was further washed in fresh electrolyte, with the purpose of removing any soluble species. The washed NVPF electrode and the extracted HC electrode were then used to assemble a new coin cell which was cycled 10 times according to the scheme on the third line of Table 2.3. After cycling the full cell was disassembled and the anode analysed using EDX.

2.1.9 Binder stability

Finally, exploring if the binder material in the HC anode contributed to cell capacity fade, PVDF binder powder was dissolved in acetone and coated on one side of a stainless steel disk. Two such disks were made and dried at 55 ° C for 24 hours and then brought into the argon filled glove-box. Thereafter, one disk was submerged in a vial containing 1 M $NaPF_6$ in diglyme electrolyte and the other in a vial containing 1 M $NaPF_6$ in EC_{50}:DMC_{50} electrolyte. Change of colour of the liquid and PVDF film was then monitored for 5 days (right part in Figure 2.5). In the next stage, the same experiment was repeated, now coating the clean side of the steel disk with Na metal. The purpose of this was to bring the binder and metal into electrical contact without touching each other directly. For the Na/binder system the change of colour of the liquid was also monitored for 5 days (left part in Figure 2.5).

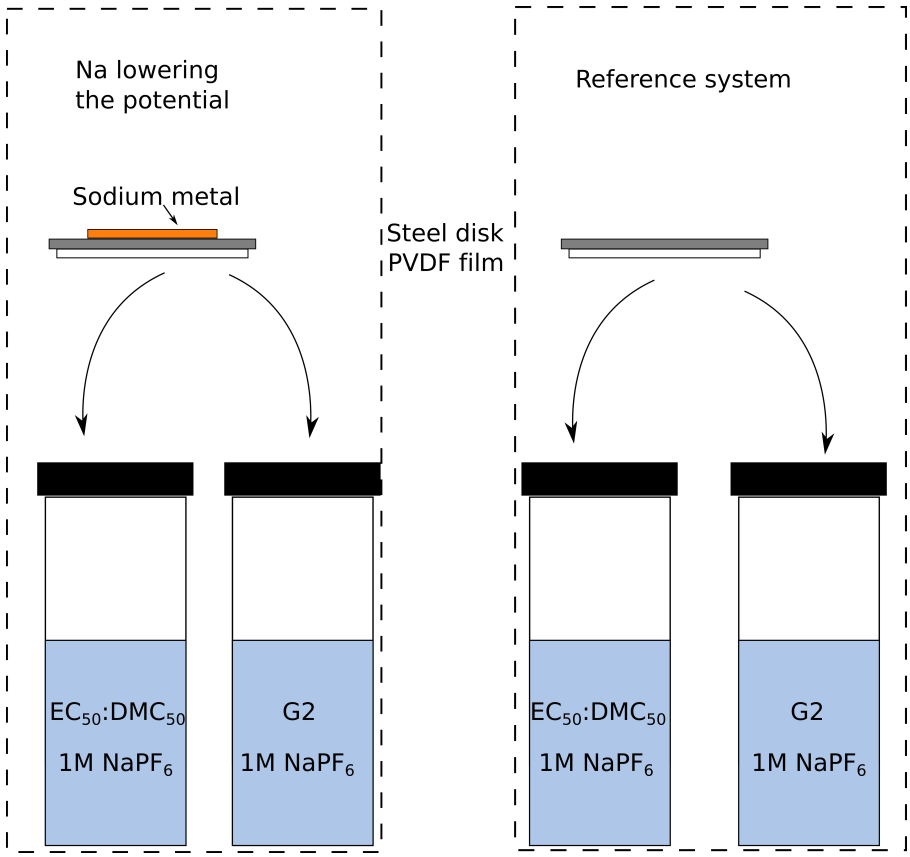

Figure 2.5: Experimental procedure used to compare degradation of binders by Na in EC:DMC- and diglyme-based electrolytes.

2.2 BIF design methodology

For the second part of this project we explored the design of a battery information format (BIF) that would be possible to employ across several battery powered applications and that could be tuned by mechanistic understanding from the lab (Paper II). To do this, we first devised a simple base case for evaluating the yearly amount of data associated with any feature set to be incorporated into the BIF. Second, we conducted a literature review and tabulated feature formats used in previous studies. Third, we devised a set of design criteria that needed to be fulfilled by a BIF for it to be widely useful. Finally, the literature study and selection criteria were used to devise the "best" BIF, according to the criteria developed.

2.2.1 Data sharing principles - the FAIR framework

The FAIR data sharing principles, proposed in 2016, were designed to formalize what is meant by "good data management" and to enable research data to be found and used also by machines (also denoted "Computational Stakeholders") [71]. While a number of domains in science have managed to establish their own frameworks for ensuring data quality, the principles strive to be generally applicable. FAIR, standing for *Findable*, *Accessible*, *Interoperable*, and *Reusable* establishes the definitions in Figure 2.6 [71]

2.2.2 Data footprint evaluation

To compare the data footprint of data generated yearly by any set of features a base case for feature data size and collection frequency had to be decided. An assumption was made that any single feature was represented by a 4 byte variable, while targets were represented by 2 byte variables. Furthermore,collection of the features and targets was assumed to happen 26 times per year (i.e. biweekly). Finally we assumed that 6 targets were collected, entirely independent on what original studies stated. Wherever it was obvious that the strategy devised above was unjust or not representative for a real life use case, the data footprint was evaluated on an individual basis, clearly communicating this was the case. For more details on individual evaluation of data footprint we refer the reader to Paper II.

2.2.3 Literature survey of feature formats

With the data footprint method we proceeded to survey literature for formats previously employed when designing targets and input features for data-driven ageing models. Both peer-reviewed and other sources were considered to achieve the broadest scope of alternatives. Studies considering health indicators (HIs), i.e. proxies for the target as the model input where excluded from the analysis, since these did not actually strive to record the usage history of a battery. For each study found, the data footprint was evaluated using the method outlined in section 2.2.2. Finally the studies found could be grouped into broader categories.

To be **F**indable:

F1. (meta)data are assigned a globally unique and persistent identifier

F2. data are described with rich metadata (defined by R1 below)

F3. metadata clearly and explicitly include the identifier of the data it describes

F4. (meta)data are registered or indexed in a searchable resource

To be **A**ccessible:

A1. (meta)data are retrievable by their identifier using a standardized communications protocol

A1.1 the protocol is open, free, and universally implementable

A1.2 the protocol allows for an authentication and authorization procedure, where necessary

A2. metadata are accessible, even when the data are no longer available

To be **I**nteroperable:

I1. (meta)data use a formal, accessible, shared, and broadly applicable language for knowledge representation.

I2. (meta)data use vocabularies that follow FAIR principles

I3. (meta)data include qualified references to other (meta)data

To be **R**eusable:

R1. meta(data) are richly described with a plurality of accurate and relevant attributes

R1.1. (meta)data are released with a clear and accessible data usage license

R1.2. (meta)data are associated with detailed provenance

R1.3. (meta)data meet domain-relevant community standards

Figure 2.6: FAIR data criteria as defined by Wilkinson *et al.* [71].

2.2.4 Scoping design criteria and attributes

To make a selection between feature categories and to be able to fine-tune any category chosen, it was necessary to define what we considered to be a "good" BIF. Hence, a set of design criteria and attributes were developed, criteria being those where a feature set could score "fulfilled/not fulfilled" and attributes being qualities of a feature set that could be evaluated on a continuous spectrum. Moving on, the feature categories were evaluated with respect to these criteria and attributes, so as to select the most compliant category. The definition of attributes were chosen with inspiration from the FAIR framework, and truly the attributes themselves where made sure to overlap with the FAIR criteria when possible. Especially criteria I1., R1., and R1.3 were adhered to, stressing that data is described with a formal, broadly applicable language, with relevant attributes that meet community standards.

2.3 Causal graphical models

In the final part of this thesis we aim to discuss a structured way of connecting mechanistic understanding of degradation to the design of a data collection strategy based on the BIF. Since this discussion builds on the framework of causal graphical models (CGMs) developed by Pearl *et al.* in the 1980s [72] we elaborate on relevant theory below.

CGMs are used to formally representing causal relationships. At the heart of this work lies the directed graph, with nodes representing measurable quantities or states and edges representing the functions mapping one node to another. Edges are *directed*, indicating the direction of interactions. For example we can model the candidate's stress during a Ph.D. defence (Figure 2.7) where we assume the work/life balance of the candidate will affect both the quality of sleep of the candidate, and the quality of the thesis. We can furthermore assume that both of these things affect the amount of stress the candidate feels at the day of their defence. Likely, there are other factors, such as outdoor temperature, affecting the quality of sleep. The direction of edges further tells us the flow of information, e.g. how quality of sleep does *not* affect the outside temperature.

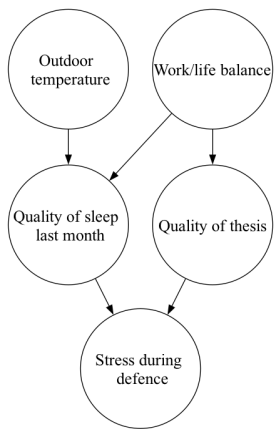

Figure 2.7: A causal graphical model of stress experienced during a Ph.D. defence.

The graph in Figure 2.7 is also an example of a directed acyclic graph (DAG) defined together with some useful terminology as.

Definition 1 *A DAG G consists of a set of vertices (i.e. nodes) V and a set of directed edges E. Each node V_i is associated with a random variable X_i. Let $i \to j$ denote an edge from vertex i to vertex j. We then call V_i the **parent** of V_j and V_j the **child** of V_i. For any directed path $i \to ... \to j$ with $k \in \mathbb{Z}_0^+$ edges between i and j, we call V_i an **ancestor** of V_j, and V_j an **descendant** of V_i.*

In a DAG, there are no paths leading from V_i back to itself. [73]

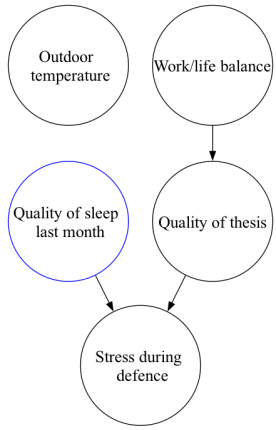

Figure 2.8: Example of an intervention, resulting in a mutilated graph.

DAGs can both be used as a modelling framework for predictions, demanding that the functions on edges are specified, but even without such specification they constitute a useful tool for communicating a data generation process and to communicate expert understanding of a physical process. Furthermore they serve as "oracles of intervention" [72], allowing for analysis how a system responds when variables are controlled by external means. This is opposed to associational/statistical knowledge about a process where one can not always conclude the effect of an intervention by just observing data of the non-intervened process [72].

In our example above, we can, for the sake of reasoning, decide to issue the Ph.D. student with sleeping pills, thus controlling their quality of sleep. This is equivalent to deleting all edges leading into the "Quality of sleep" vertice. The controlled node, indicated by a blue outline, now lacks any parents. This is opposed to when we just observe data from the original process and try to draw conclusions about sleep quality's impact on thesis defence stress.

Chapter 3

Results and discussion

In the following chapter we present the major results in Paper I and Paper II and elaborate on how they can be integrated into a common flow for designing battery field data.

3.1 Discovered degradation pathways

Understanding of potential routes for degradation aids when diagnosing field-operated commercial cells and can further provide guidance when trying to tune a BIF. Here we present the degradation pathways and lack thereof discovered for the SIB investigated in Paper I.

3.1.1 Electrolyte stability and SEI growth

Since we mainly focused on the electrolyte in Paper I, the first two ageing mechanisms (ref. Figure 1.4) investigated were electrolyte stability and SEI formation. To probe oxidative stability, LSV sweeps were made on half cells with various positive electrode substrates employing the 1 M $NaPF_6$ in diglyme electrolyte. Substrates affect the oxidation potential and can introduce a shift from *ca* 4.4 V to *ca* 4.6 V vs. Na^+/Na° (Figure 3.1, left). Furthermore, the NVPF voltammogram shows evidence of NVP contamination in the NVPF, in the form of a peak at 3.4 V (Figure 3.1 left, inset, purple line), the exact Na^+ extraction potential in NVP [74], [75].

No oxidation was observed below 4.4 V, i.e. 0.3 V above the second extraction peak of the NVPF cathode material at ca. 4.1 V. Both the substrate dependency and the upper limit of 4.4 V are relevant to consider when tracking degradation in the field, so as to not exceed these limits and cause unwanted electrolyte decomposition. The possibility of NVP contamination and associated defects is also interesting since it might pose a risk for transition metal dissolution.

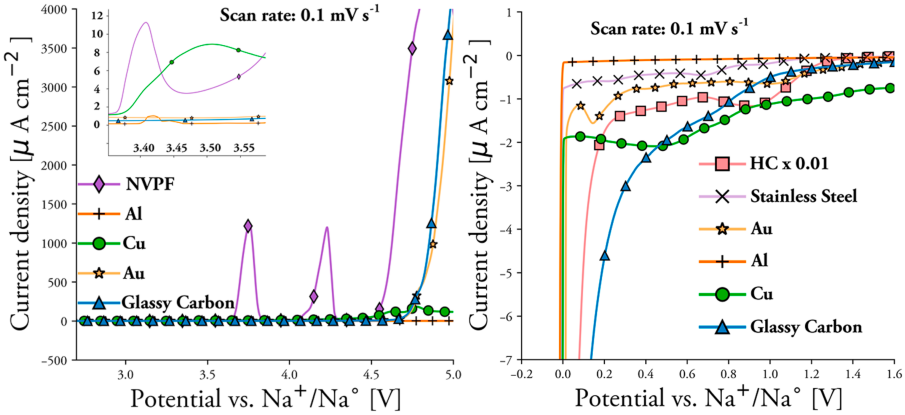

Figure 3.1: LSV of 1 M $NaPF_6$ in diglyme vs multiple counter electrodes probing electrolyte oxidation behavior (left) and reduction behaviour (right). Please note the 0.01 multiplying factor for the HC curve.

For reductive stability of the electrolyte we also observe a substrate dependence, albeit with much lower current densities for all substrates. The LSV indicated electrolyte reduction only below 0 V for the non-electrochemically active substrates (Figure 3.1, right), likely due to Na plating [19]. The small reductive currents observed already above 1.2 V for all substrates except Al are solvent independent and have previously been assigned to parasitic reactions involving H_2O or O_2 contaminations or possibly slow electrolyte reduction[62].

To further probe the presence of any SEI formation, EIS measurements were done on symmetrical Na cells. The shrinking of semi-circles with time in the Nyqvist plot (Figure 3.2) indicates that no continuously growing SEI is present. Alternatively, the SEI might be growing but is so permeable that ion conduction and surface kinetics are not impacted significantly. In Paper I we further discuss the possible reason for the shrinking of semi-circles.

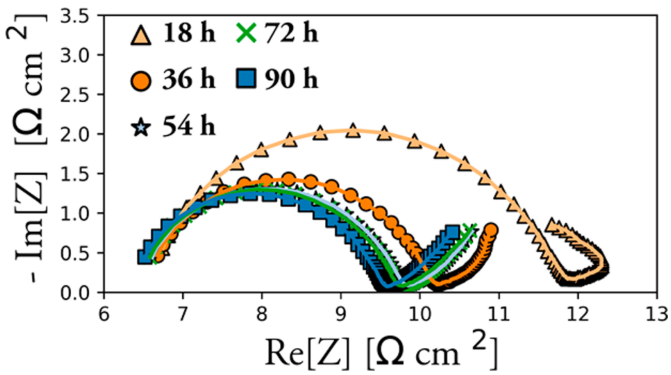

Figure 3.2: EIS spectra of symmetrical Na|1 M $NaPF_6$ in diglyme|Na cell at different times of rest after assembly.

Electrolyte reductive stability was further investigated by liquid GC/MS analysis, conducted on separators from cycled full cells. The lack of observable peaks in the GC data (Figure 3.3), other than the washing compound and the diglyme, indicates no soluble liquid degradation products.

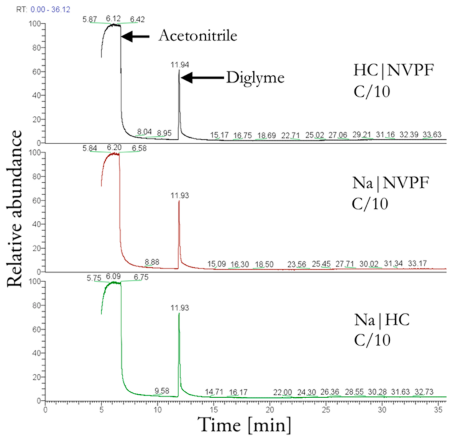

Figure 3.3: Liquid injection GC data for cycled separators.

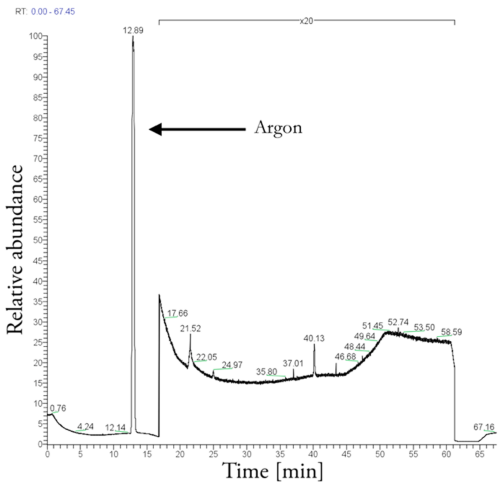

Figure 3.4: GC data of gas when storing Na metal in diglyme. A multiplication factor of 20 has been applied between 15 and 65 min.

Similarly, GC/MS conducted on ambient gas when submerging sodium metal in the electrolyte did not indicate any gaseous degradation products to be released (Figure 3.4). The combination of gas and liquid-phase GC/MS data don't completely exclude the possibility of electrolyte reduction, since there could still be (semi-) solid compounds formed that are insoluble in diglyme (see reaction pathways in Paper I, SI). However, this evidence *together* with LSVs,

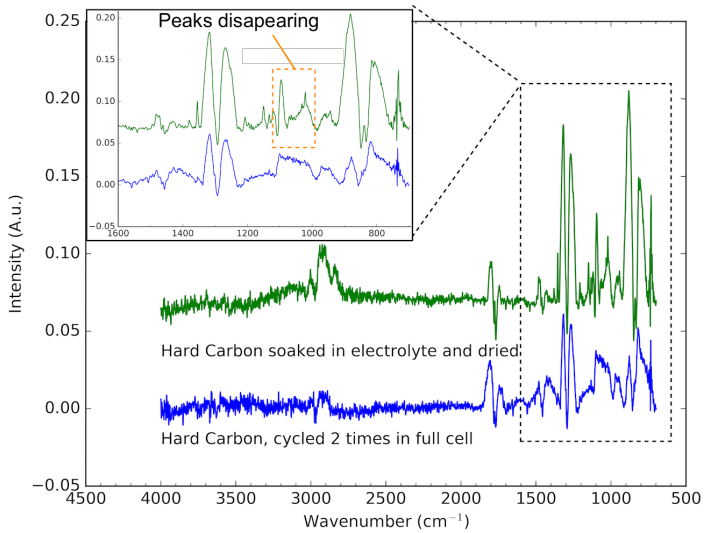

Figure 3.5: FTIR spectra of cycled and pristine HC anodes.

EIS and the complementing FTIR analysis of cycled cell anodes (Figure 3.5), lacking any signatures of degradation products, all corroborate the hypothesis of a lack of electrolyte degradation or SEI formation.

Given the evidence that 1 M $NaPF_6$ in diglyme was stable against reduction on Na surfaces and with HC anodes, several GCPL-cycling tests were conducted. We refrain from discussing the results in detail and refer the reader to Paper I for the full analysis. Instead, as a briefer summary, we first note that both half cells suffer from an initial irreversibility: the 3% for NVPF, probably related to the NVP contamination undergoing an irreversible phase transition at the high potentials experienced, and 23 % for HC attributed to some initial parasitic process consuming Na. With previous result on (lack of) SEI formation we are hesitant to attribute the irreversibility on HC to electrolyte reduction even if this is the conventional hypothesis [59]. What further stands out is that the first cycle irreversibility is significantly larger for the diglyme (ca. 23%) than the equivalent alkylcarbonate (ca. 17%) based electrolyte. This is surprising given the relatively thick SEI formed by alkyl carbonate based electrolytes [76].

Studying the continuous (normalised) capacity evolution of half and full cells for the 2^{nd} to 16^{th} cycles we can further observe that the HC, as compared to NVPF, has a significantly higher capacity loss already at the end of this short interval (ca 3%), with no observable trend of stabilizing (Figure 3.6, diamonds), even though both half cells suffer from a similar coulombic efficiency of 99.5 % . As a comparison, commercial cells are expected to retain $> 80\%$ capacity after > 1000 cycles, translating into a loss of < 0.3 % after 15 cycles [11]. This indicates that in the HC electrode we are experiencing LAM and possibly LLI at the same time, while in NVPF we are either experiencing a mimimal amount of LAM, and/or electrolyte oxidation.

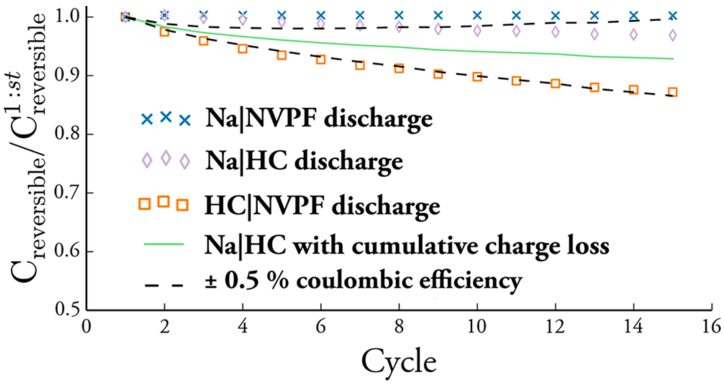

Figure 3.6: Capacity relative to the second cycle (i.e. first reversible cycle).

The issue of the compatibility between HC and the electrolyte is further corroborated in the same graph when comparing the results to the full cells. If using the coulombic efficiency from the Na|HC cell and accumulating the capacity loss, the full cell performance is matched within a ± 0.5 % window, the full cell having only a 99 % coulombic efficiency. Finally, tests using a different anode (NVP) with a higher working potential further confirmed that when excluding the HC anode, cells significantly stabilised in cyclability (Figure 3.7, NVP|NVPF). Tellingly, using NVP in the cathode configuration (HC|NVP), thus lowering the risk of electrolyte oxidation, also yields cells with a capacity fade similar to that of the full HC|NVPF cells.

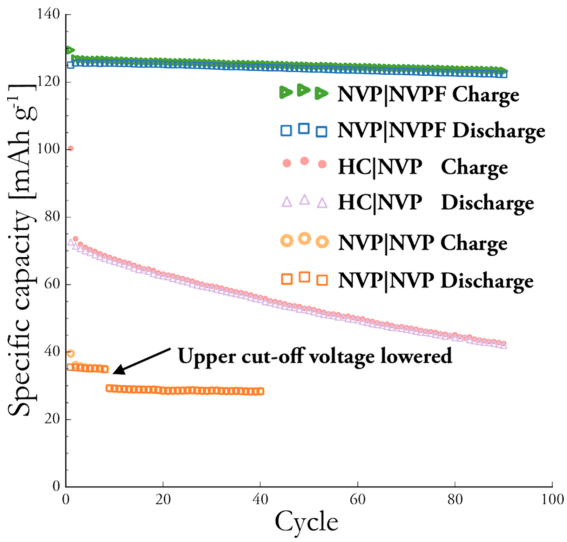

Figure 3.7: Cycling performance with different anodes. Please note that for the NVP|NVP cells the anodic capacity is used, while for both the HC|NVP and NVP|NVPF cells the cathodic capacity is used.

3.1.2 Binder stability

Given that the underlying mechanism for the poor performance of HC in full cells remained elusive, including the lack of detectable SEI formation, we shifted focus to other degradation mechanisms. Upon testing the binder (PVDF) compatibility with Na-metal in both 1 M $NaPF_6$ in EC_{50}:DMC_{50} and 1 M $NaPF_6$ in diglyme we found a significant discoloration and deterioration of PVDF happening in the latter, but not in the former (Figure 3.8). This indicates that diglyme as a solvent has the property of allowing PVDF reduction.

Binder reduction could both be directly and indirectly responsible for the initial and continous irreversibilities seen in HC half cells and NVPF|HC cells. The direct effect can be evaluated assuming that the binder makes up 4 - 6 % of the anode, weighting 4.9 mg and that active material makes up 90% of the cathode, weighting 9.6 mg. The resulting ratio between F-C bonds and available Na is approximately 1:6 - 1:4 ((C-F):Na), not matching the 30 % initial irreversibility in full cells and half cells. The indirect effect of a weakened binder is likely disconnection of the active material, contributing both to the initial and continuous irreversibility.

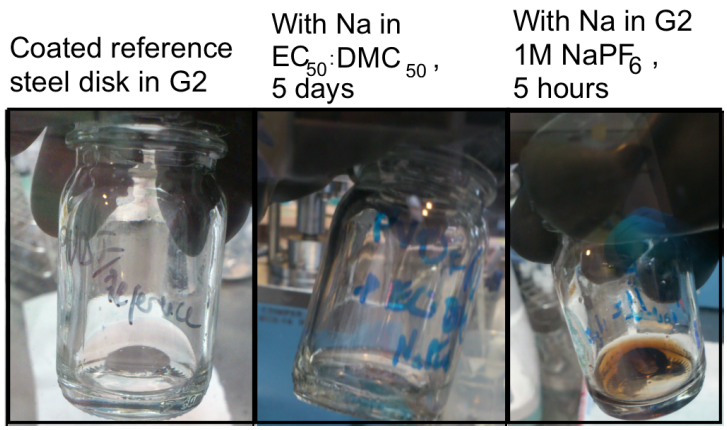

Figure 3.8: Ocular inspection of binders in different electrolytes before and after being subjected to Na.

3.1.3 Transition metal dissolution

A final degradation mode we investigated was the risk of transition metal dissolution, an issue often enountered in LIB cathodes containing manganese. Probing HC anodes cycled in full cells with our diglyme electrolyte using EDX inside of a SEM, we indeed observed peaks relating to Vanadium (Figure 3.9) both from pristine cells and cells where the NVPF electrode had been removed, washed and reassembled into new cells. This points towards another degradation mode leading to continuous capacity loss, where V-ions are being shuttled from the cathode to the anode, where they deposit as vanadium metal, consuming Na inventory in the process. Degradation by transition metal dissolution was further corroborated by observing that the HC electrodes had a bluish hue after cycling (Figure 3.10), indicative of V^{4+} ions [77].

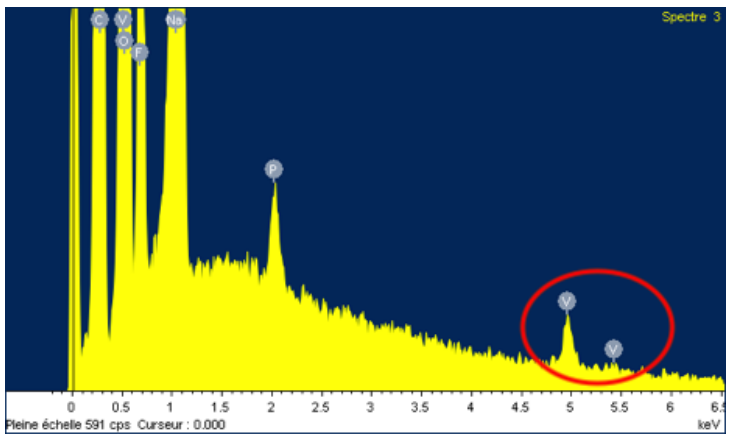

Figure 3.9: EDX spectra from cycled HC anodes.

Figure 3.10: Hard carbon electrodes before and after cycling.

3.2 The BIF

Given that it is neither practically, nor economically feasible to conduct the experimental campaign in Section 3.1 on a fleet of battery packs and cells, a different methodology has to be used to record data and forecast degradation in the field. A BDT provides this opportunity but to fully realise its potential, the right information, including features and targets, has to be collected. In this section we discuss results from Paper II and the effort to suggest a widely applicable standard for a battery information format (BIF) for BDTs.

3.2.1 Results of meta-analysis of targets and features

Given the multiple attempts made to perform data-driven forecasting of degradation in batteries, our first step in Paper II to develop a BIF standard was a meta-analysis of previous work. Forecasting SOH, RUL, and possibly SOS, involves deciding on a desired model output(s), consisting of a combination of performance metrics. For targets we found that mostly those relating to capacity have been used, either predicting absolute values, capacity loss (Figure 3.11, ΔQ) in a predefined usage window (Figure 3.11, "UW"), forecasting of the EOF or knee-point, i.e. the event where onset of rapid non-linear loss begins [78]–[84]. A few studies have focused on the resistance, including predicted pointwise resistance, knee point, and the EOF (Figure 2, purple line) [85], [86].

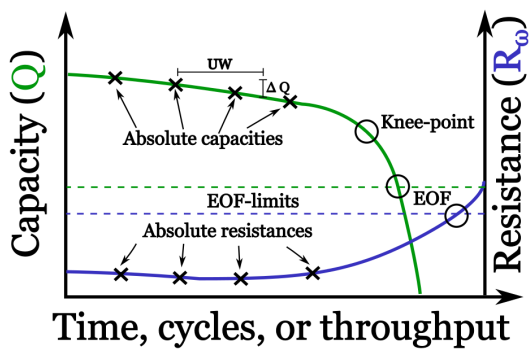

Figure 3.11: Most common targets proposed in literature.

Further results from our meta-analysis indicate four main categories employed (Table 3.1): Incremental capacity curve derived features, Event counting, Histograms, and Semi-empirical. In Paper II we explain these thoroughly and tabulate several common metrics reported for feature type, size, data collection strategy, and reported accuracies in predicting battery health. Here we instead settle for a summary version of that tabulation (Table 3.1), where the annual data footprint has been estimated using our data footprint base case (ref. Section 2.2.2). It is not obvious that any feature category has better performance or practical applicability from this analysis alone, calling for the development of more detailed selection criteria.

Feature type	**Typical annual data footprint [kB]**	**Reported RMSE in Q [%]**	**Reported RMSE in RUL [%]**	**Sources**
Incremental capacity curve	104	N/A	11	[79], [84], [87]
Event counting	79	1.7-10	N/A	[88]
Histograms	16-36	1-11	1-3	[24], [79], [81], [89], [90],
Semi-empirical	0.4-0.5	1-2.3	3-5	[82], [91]

Table 3.1: Summary of features and targets employed in literature. For a more detailed view we refer the reader to table 1 in paper Paper II.

3.2.2 Design requirements

To guide our selection of good candidates for a BIF we arrived at a set of selection criteria and requirements : **Data Footprint** (DF), **Interpretability** (I), **Accessibility**, **Predictive Power** (PP), and **Reusability** (R). The criteria, summarised in the green box below, account for both qualitative and quantitative aspects of data collection and lifetime modelling of LIBs and SIBs.

To yield a low **d**ata **f**ootprint :

DF 1. The number of bytes collected annually are kept at a minimum.

DF 2. The number of redundant features/variables are low.

To be **I**nterpretable:

I 1. Features and targets allow for physical interpretation, making it possible for humans to understand them.

I 1.1 Features make it possible to propose alternate scenarios still relevant for the application.

I 2. Features relate to causally relevant mechanisms that have impact on the targets.

To be **A**ccessible:

A 1. Features and targets can easily be collected from an engineering perspective.

A 2. Artificial variability in features introduced due to variation in definitions or implementation of collection software is low.

To have **P**redictive **P**ower:

PP 1. Features are accurately predicting the target.

To be **R**eusable:

R 1. Features and targets collected in one application can be transferred to the analysis and modelling of other applications.

R 2. BIF data is complemented with adequate metadata.

By **data footprint** we consider how many bytes of data that need to be transferred annually for a given feature set. A low footprint is desired, reducing transmission, processing, and storage of data, each driving cost and complexity. Furthermore, the possibility of fewer redundant variables in the target and feature set improves training speed and robustness by avoiding overfitting.

By **interpretability** we mean the degree to which features allow for a physical interpretation, making it possible for humans to understand them and propose alternate scenarios still relevant for the application [24]. The mean SOC is easily interpretable as the mean state of lithiation, while aggregated statistics, such as higher order moments (e.g. kurtosis or skewness) of residence time histograms, are harder to interpret. The interpretability should be as high as possible, acknowledging it often comes at the expense of data footprint.

By **accessibility** we mean the ease with which a feature can be collected from an engineering perspective. Accessibility can be impaired by difficulty to observe the quantity of interest or when very specialized and expensive sensors are needed. For example optic fibres used to sense the state of lithiation in the anode have been proposed but the engineering limitations pose a challenge for mass-market implementation of such techniques [92]. Accessibility further denotes the risk of artificial variability introduced due to variation in definitions or implementation of collection software. As an example, aggregated features or those relying on a state estimates depend on the battery manufacturer's implementation of the underlying algorithm. Such variability hides "true" estimates and lowers accessibility. Accessible features and targets are unanimous and can easily be read out with low risk of artificial variability.

By **predictive power** means how accurately a feature set allows prediction of targets. The main prediction targets and modelling strategies are mentioned above in section 3.2.1, but there are other less explored targets worth predicting as well, including fast/slow dynamics resistance, available useful energy, and SOS. A BIF should yield predictions with high accuracy and reliable error bounds for as many of these targets as possible.

Finally, **reusability** is defined as the ease with which features collected from one application could be transferred to another application, especially useful if the same (type of) cells have been used. However, data could partially be reused for initialization of ageing models also for other cases, given that it has been collected in such a way that the datasets can be reused – either directly or through proper resampling. An important aspect of reusability not covered in Paper II includes the inclusion of proper metadata. To maximise utility for a user of data and provide a meaningful way of data interpretation, details about cell chemistry (anode, cathode), supercell capacity, physical cell format, and the number of physical cells per supercell should be included. If possible, the voltage limits as specified by the cell manufacturer should be also be provided to guide interpretation.

3.2.3 Feature and target selection

For targets to be collected in the BIF, we include both instantaneous total capacity (Q_{tot}), and equivalent DC resistance at 20°C, 50 % SOC and timescales 1s and 10s (R_1 & R_{10}). We define R_x as

$$R_x = \frac{\Delta V_x}{\Delta I_x}, \tag{3.1}$$

where I_x is a 1C discharge current pulse applied for x seconds and V_x is the voltage difference between time t and time $t + x$. Furthermore, to communicate the quality of the target estimates (only estimates are available in this case, and never direct measurements), standard deviation σ for each estimate is included in the BIF. Our final set of targets then becomes:

$$\begin{array}{ll} Q_{tot} & \sigma_Q \\ R_{1s} & \sigma_{R_{1s}} \\ R_{10s} & \sigma_{R_{10s}} \end{array}$$

Continuing with the features, we apply our selection criteria on the categories observed in literature and give them a *Low, Medium, or High* score in each criteria (Table 3.2). Incremental capacity curve features score low on both data footprint, Interpretability, and Accessibillity. These features require the whole incremental capacity curve to be captured every time the feature is to be recorded, thus impacting *DF* and *A* criteria. Furthermore, for the Interpretability, it is not entirely clear how to modify the curve, nor it's mean, variance, and kurtosis, to propose an alternate scenario relating to a change in operational pattern of the battery.

Feature category	**DF score**	**I score**	**A score**	**PP score**	**R score**
Incremental capacity curve-derived	Low	Low	Low	Unknown	Medium
Event counting	Medium	High	Low	Unknown	Low
Histograms	High	High	Medium	Unknown	High
Semi-empirical	High	High	Medium	Unknown	High

Table 3.2: Results from scoring of feature categories with respect to design requirements

As for the other feature categories they rank similarly in data footprint with significant flexibility in how much data to collect but with Event counting scoring slightly lower in accessibility due to it being non-trivial to define an

event, which will introduce artificial variability into the feature. Also for Event counting, the reusability score will be low, since for some applications certain events never occur, e.g. a "driving" event never happens in a BESS system. For histograms and semi-empirical features we assume they are equal in all aspects considered. Histograms, however, offer a greater flexibility and can capture a richer picture of the battery usage history.

As a final comment about the predictive power, here judged to be unknown for all feature categories, studies predicting capacity (change) or EOF have demonstrated an RMSE of 1-10%, but the datasets used to conduct these studies lack the richness experienced in real life applications. This implies that it is impossible to draw conclusions about how well results generalize and thus to judge the predictive power for capacity and resistance prediction. Given that residence time-counting histograms offer more flexibility and higher granularity for capturing battery usage, this is the feature category we decided to proceed with. They are furthermore attractive from a causal standpoint since they contain the necessary components to describe kinetics for parasitic reactions; both information about the time spent in a certain condition, and the nature of the rate-determining conditions (I,V,T) can be simultaneously communicated.

3.2.4 Specification of histograms

Histograms include features that count the distribution of some aspect of the battery's usage history and is one of the most frequently used features observed in literature. Multidimensional histograms with 1-3 axis dimensions and time as counting dimension have often been used, resulting in so-called "residence-time counting" histograms [24], [79], [81], [89], [90], [93]. Deciding to proceed with histograms as the basis for the feature set specified by the BIF, we specify histogram axis dimensions.

Axis dimension	**Stressors captured**
I vs. V	High (cathode) voltage / low anode voltage, high current
i vs. T	High current at low temperature, high current
V vs. T	High (cathode) voltage / low anode voltage, high temperature
V vs. i_{MA30s}	High (cathode) voltage /low anode voltage, high sustained current
SOC vs. T	High/Low mean lithiation, high temperature
SOC vs. i	High/Low mean lithiation, high current
SOC vs. i_{MA30s}	High/Low mean lithiation, high sustained current

Table 3.3: Axis dimensions for BIF histograms.

To allow for a rich enough data we include including voltage, temperature, current, SOC, and a 30 s moving average of current (i_{MA30s}) to be used (Table 3.3). The latter is defined as

$$i_{MA30s} = \int_{t-30}^{t} i(\tau)d\tau, \tag{3.2}$$

and captures sustained current, something otherwise lost when forming histograms, resembling the 3-minute RMS-feature used by Zhang et al. [81] but accounts for directionality of the current (charge and discharge are separated) making it more suitable to capture local overcurrent and over/underpotential conditions. In Paper II we further explore the accessibility of each axis dimension but omit it here for the sake of brevity.

3.2.5 Design details - maximising histogram reusability

Based on selected targets and features, we now proceed to define units and binning strategy. This is done to fully specify the BIF and satisfy the reusability criterion. For the same reason, quantities observed across applications should be of similar magnitudes and bins should satisfy necessary overlap criteria – so that fine-grained and course-grained histograms can be compared.

Quantity/ Dimension	V/V	I/C-rate	i_{MA30s} /C-rate	SOC/%	T/°C
Alignment point	3	0	0	50	15
Base layout spacing	0.5	1	1	25	10
Bin aggregation dimension	Minutes				
Collection frequency	Biweekly				
Bin refinement divisor	2				

Table 3.4: Hyperparameters for BIF design

First, we consider units (Table 3.4, first row), requiring that current is expressed as a directional C-rate, i.e. current is normalized by the mark-plate capacity of the given (super) cell. Voltage (in Volts), and temperature (in °C) stay within the same order of magnitude/range meaning no normalization is needed. For histogram count dimension we suggest using minutes to allow for capture of rare conditions. Collection frequency is further set to bi-weekly, corresponding to one where degradation can be observed between samples, when cells are subject to the harshest operating conditions [87].

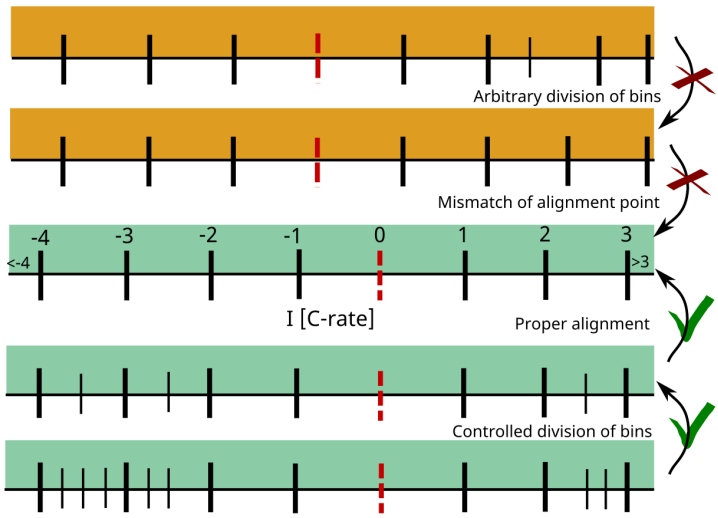

Figure 3.12: Proposed histogram bin construction and impact on reusability.

Second, there is a need to establish an alignment of the histogram bin edges (Figure 3, red line), requiring the specification of where to put at least one edge. Without alignment there is a risk of offset between data collected from different cells, impacting the reusability. Alignment points should be chosen such that they cover most battery cell use cases since all data formats will need to include this.

Third, for the data format to allow for histogram down-sampling, we suggest using a base partitioning scheme for the bins – from here on called "base layout", and rules for refinement. A base layout (Figure 3.12, middle bin layout) is the coarsest bin size allowed and it needs to allow for sufficient data minimization while being detailed enough to enforce reusability of data. For simplicity, we propose using an evenly spaced binning, starting from the alignment point and continuing as far as is required by the application at hand. We note, however, that the base layout could be designed with non-uniform bin partitions but leave this for future work to explore. Allowing for design freedom, any application should be allowed to split the base grid into further partitions. However, to maintain reusability, any partitioning scheme should only split existing bins in two (Figure 3, lower green bin layouts). A divisor of 2 is selected as it impacts the data footprint the least.

Fourth, the last bin on each side of the histogram should be required to capture any remaining data "falling off the edge" (Figure 3.12, edges of bin layouts). Finally, the collection frequency is specified, here suggested to be an aggressive base-case of biweekly collection, leaving the exact collection frequency as a design parameter, but requiring it to be an integer multiple of the biweekly interval. By doing so, transferability is achieved. In Table 3.4 we summarize our full proposal of BIF design hyperparameters.

3.3 Bridging mechanism and BIF tuning with CGMs

With the introduction of a BIF we now proceed to approach the question of how to use mechanistic understanding of ageing from the lab into the tuning of a lean data collection strategy possible to use in a field application. This is done by formulating our mechanistic knowledge as a CGM and then using the CGM as a guide when designing the binning scheme of the BIF.

3.3.1 Encoding our undestanding of the SIB in a CGM

Looking at a generic CGM of battery ageing (Figure 3.13). This is a merged subset of the information shown in Figure 1.4, where we consider five failure modes: Electrolyte decomposition, SEI formation and destruction, Binder decomposition, Transition metal dissolution (TM dissolution), and Current collector corrosion (CCC).

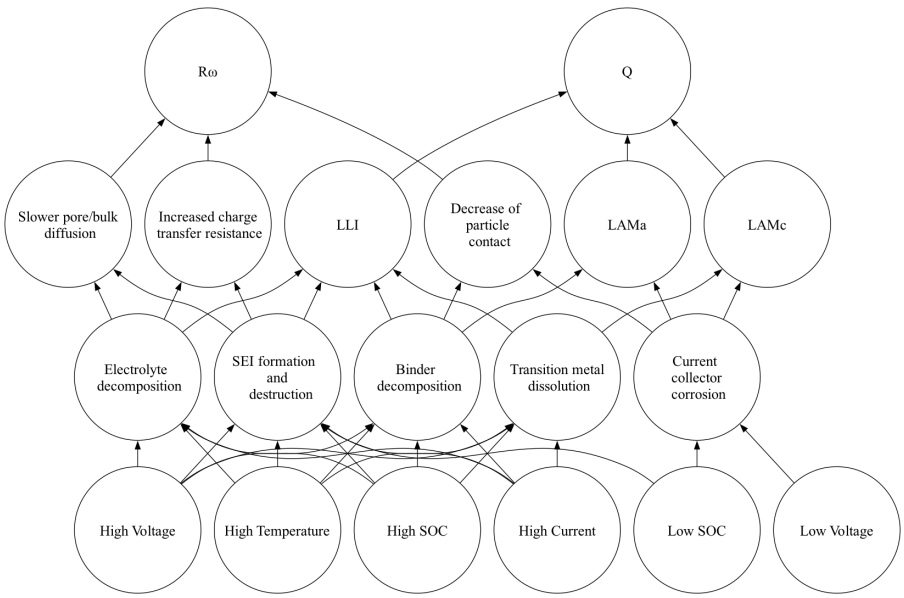

Figure 3.13: Generic CGM for five battery failure modes.

For most LIB chemistries, these five modes will not be equally relevant (Figure 3.14). Especially, we assume that binder degradation plays a negligible role for LIBs. Also transition metal dissolution can be expected to be limited in chemistries with little Mn in the cathode, such as LFP or NMC111 even though not completely accurate for the latter [94], [95]. Regular LIBs, however, will suffer from SEI formation and non-SEI forming breakdown of the electrolyte. Also, CCC will be an issue at low cell voltages and SOCs.

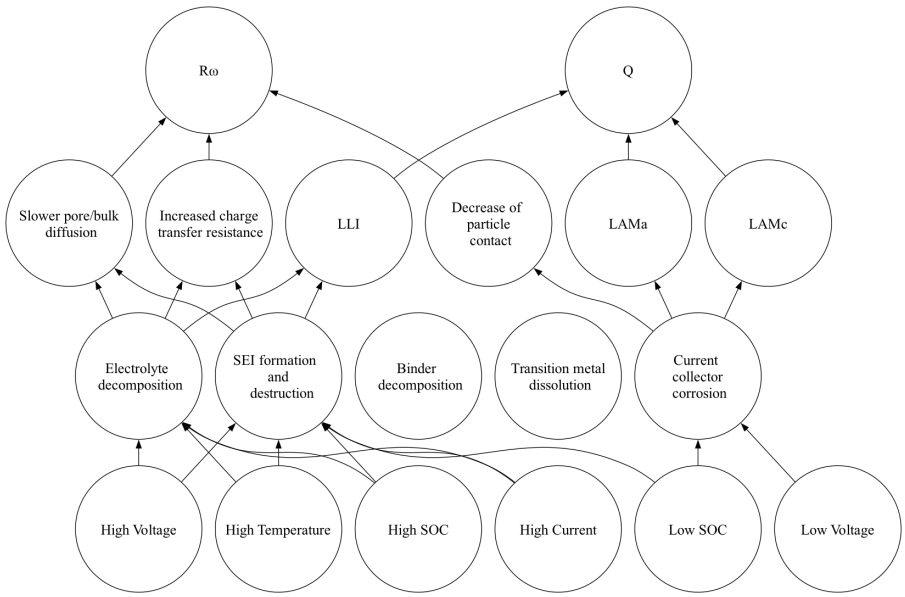

Figure 3.14: CGM for a LIB cell, lacking TM dissolution and binder degradation.

For the investigated HC|1 M $NaPF_6$ in diglyme|NVPF cell we instead have an almost opposite situation in the causal structure (Figure 3.15) where our study shows little evidence of electrolyte breakdown or SEI formation. This is equivalent to mutilating the generic graph to remove any paths involving these two mechanisms. We still let the nodes relating to increased charge transfer resistance and slower pore/bulk diffusion remain connected to the observed quantities Q and R, to highlight that these could potentially be altered by other degradation mechanisms, not included in the CGM.

Instead we have observe clear evidence of both binder degradation and TM dissolution. Furthermore, SIBs are able to utilize aluminum current collectors due to Al not alloying with Na. The stability of Al at higher potentials means that SIBs can be discharged to 0V without detrimental CCC [96].

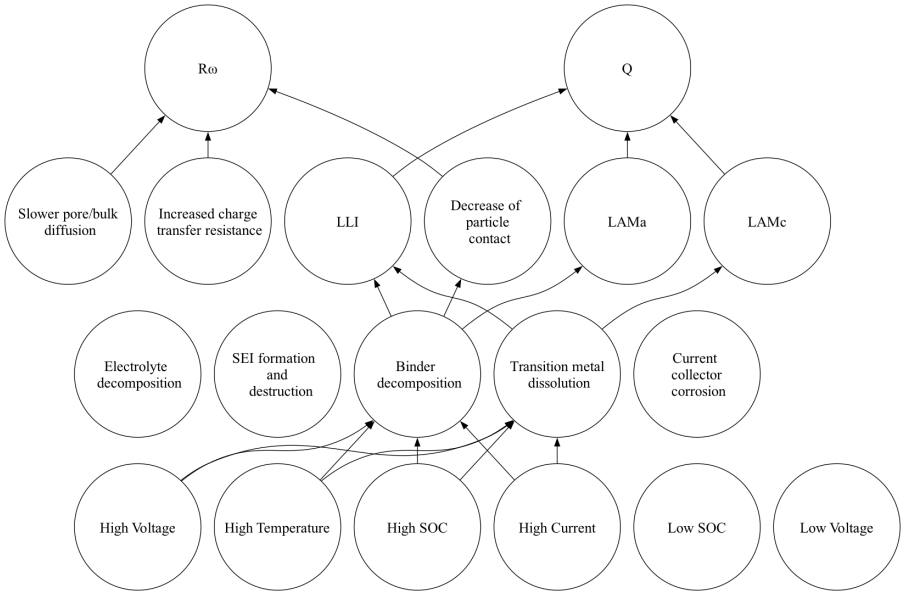

Figure 3.15: CGM for the HC|1 M $NaPF_6$ in diglyme|NVPF cell.

3.3.2 A BIF for SIBs with a diglyme electrolyte

Given the understanding of degradation mechanisms documented in the CGM in Figure 3.15 and, for illustratory purposes, assuming this is the complete picture of degradation, we now proceed to specify a information collection strategy compatible with the BIF. Our aim for this strategy will be to minimize the data footprint while still being able to capture enough information about the cell usage to model the degradation and trajectory of targets.

First, we note that the lack of CCC means we don't need to consider the low voltage region. Thus, we design the voltage binning scheme with 3 V, the alignment point, as the lowest point. The BIF then tells us we need to add bin edges in increments of 0.5 V. Since the max cell voltage is 4.3 V and transition metal dissolution likely happens at these higher voltages, we are keen to capture the higher voltage region with higher granularity, given that on it we first add the points 3, 3.5,4,4.5 and then use the division rule to split the higher bins so that edges 4.25,4.3125,4.375 are added giving us 6 bins in total (Figure 3.16, first axis). Due to the same reasons we limit the SOC bins so that all residence time below 50 % is aggregated while at higher SOCs granularity is higher (Figure 3.16, second axis).

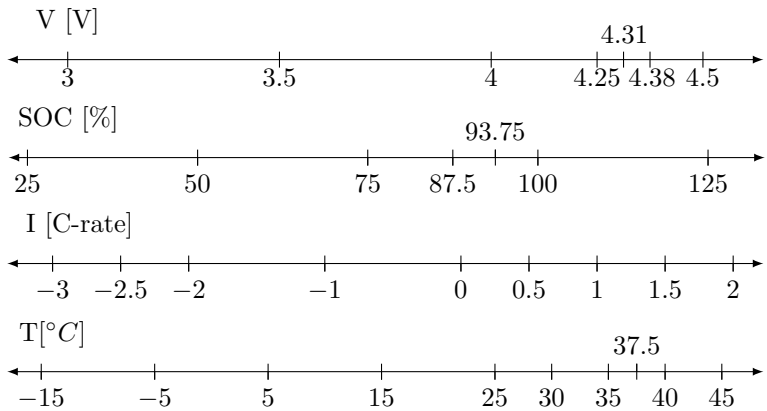

Figure 3.16: Binning scheme for voltage, SOC, current, and temperature for our data collection strategy design for the diglyme-based battery.

Proceeding with current, we assume the cells will operate at max 3 C discharge and 2 C charge. Thus, we add points every 1 C between -3 and 2 C. Since the lack of SEI and the previously reported power capability of the HC|NVPF system [97] implies fast charge transfer dynamics throughout the lifetime of the battery, we do not aim for high granularity for the current. This allows us to only split the lowermost bin in two to understand how much discharge happens above 2.5 C, remembering that the last bin captures everything falling of the edge. We also split the two charging bins in two, giving a slightly more detailed picture with a total of 8 bins (Figure 3.16, third axis). For the reasons of high power capability we can also use this binning scheme for i_{MA30s}.

As for temperature, the CGM tells us it is a stressor that will still impact ageing. This will likely be the case for any chemistry, since higher temperatures tend to increase calendar ageing of materials [98]. Assuming 40 degrees to be the max temperature and knowing that degradation is accelerated at higher temperatures we add extra granularity in this region, ending up with 9 bins in total (Figure 3.16, fourth axis).

3.3.3 From lab to field and back again

Having selected the binning scheme, we now have a fully specified data collection strategy for our HC|1 M $NaPF_6$ in diglyme|NVPF cell. Including the six targets specified by the BIF (Section 3.2.1), the binning scheme gives rise to a data footprint of 39 kB/year if we account for all histograms in Table 3.3.

This memory-efficient data collection strategy can now be implemented in an application. Taking the fictional case of an SIB electric motorcycle (Figure 3.17), the data collected will have a causal relationship to any degradation observed and can be used to train a model for forecasting SOH decline. The interpretable nature of the data further provides the opportunity to identify blind spots that are not currently explored by the fleet. For our motorcycle fleet, we may for example identify a lack of fast charging (> 1C) at all SOC-levels (Figure 3.17, top of the histogram on the right side). Lab measurements can then be used to fill this gap and report data back on the same format to complement model training. Taking it a step further, the process of filling blind-spots may be automated using a Bayesian optimization, similar to that used by Attia *et al.* [54].

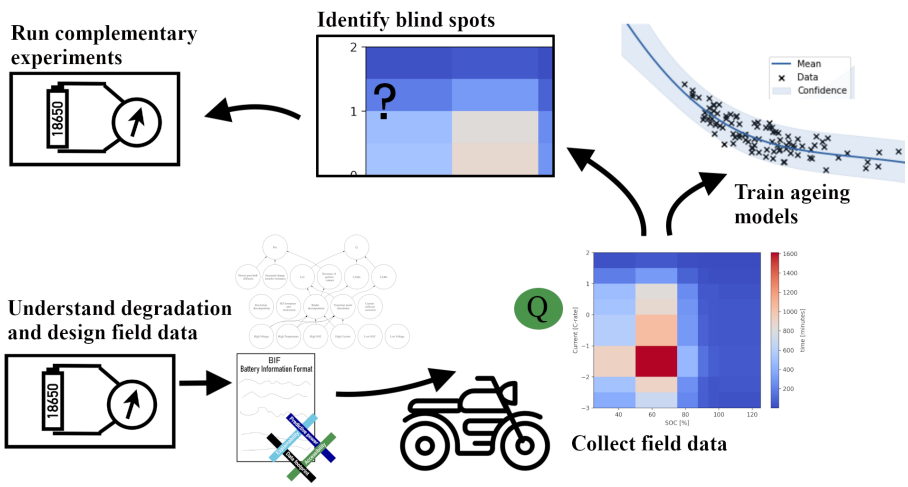

Figure 3.17: Closing the loop between lab and field.

Chapter 4

Conclusions and outlook

This thesis has studied degradation at the materials level in a SIB cell (Paper I) employing diglyme as an electrolyte. By extensive characterisation we conclude that diglyme tends to suppress or completely avoid any SEI growth while still resulting in large capacity fade when used with HC anodes. Furthermore we have shown how it is possible to design a BIF based on 2D histograms for ageing prediction that respects necessary design requirements (Paper II) and the FAIR principles.

We further conclude that any such format should still rely as much on mechanistic understanding of battery failure modes and the memory constraints of BMSes, as it does on the limited empirical evidence available in the academic literature. We finally conclude that GCMs allows for a structured way to to tie the material and fleet levels together. This is done by allowing lab data to guide what edges to include or remove in the degradation GCM. The GCM can then be used with the BIF and tuning the histogram binning scheme when devising a data collection strategy for the field.

Looking forward, we suggest that the unknown mechanism for capacity fade observed in Paper I is uncovered by further investigation. Specifically it is important to develop the understanding of binder degradation and possibility of Na^+ trapping in the anode when using diglyme-based electrolytes. For the BIF, we acknowledge the need for further validation and optimization, preferably on large scale scale dataset. However, given the connection to mechanistic understanding and the ample possibilities of designing histogram axis dimensions, binning, and collection frequency, we are confident that the BIF will provide a useful starting point for future BDTs when balancing the trade-off between data footprint and predictive power.

We finally suggest that any OEM or battery system operator that have not yet devised a data collection strategy, should consider using (a subset) of the BIF features and targets presented above to not lose valuable insights. We also stress that it is imperative that the, so far fragmented, battery data landscape gets mended, allowing society to truly leverage the possibilities that BDTs provide to strengthen the resource efficiency of LIBs and SIBs.

Bibliography

[1] N. Popovich and B. Plumer, 'How electrifying everything became a key climate solution,' *The New York Times (Web version)*, Apr. 2023. [Online]. Available: https://www.nytimes.com/interactive/2023/04/14/climate/electric-car-heater-everything.html (visited on 23/08/2024) (cit. on p. 1).

[2] F. Hedenus, U. M. Persson and F. Sprei, *Sustainable development : nuances and perspectives*, First edition. Lund: Studentlitteratur, 2018, ISBN: 9789144129068 (cit. on p. 1).

[3] M. Chordia, A. Nordelöf and L. A. W. Ellingsen, 'Environmental life cycle implications of upscaling lithium-ion battery production,' *International Journal of Life Cycle Assessment*, vol. 26, pp. 2024–2039, 10 Oct. 2021, ISSN: 16147502. DOI: 10.1007/s11367-021-01976-0 (cit. on p. 1).

[4] M. Chordia, S. Wickerts, A. Nordelöf and R. Arvidsson, 'Life cycle environmental impacts of current and future battery-grade lithium supply from brine and spodumene,' *Resources, Conservation and Recycling*, vol. 187, p. 106 634, Dec. 2022, ISSN: 0921-3449. DOI: 10.1016/j.resconrec.2022.106634 (cit. on p. 1).

[5] S. Wickerts, R. Arvidsson, A. Nordelöf, M. Svanström and P. Johansson, 'Prospective life cycle assessment of sodium-ion batteries made from abundant elements,' *Journal of Industrial Ecology*, vol. 28, pp. 116–129, 1, ISSN: 1530-9290. DOI: 10.1111/jiec.13452 (cit. on p. 1).

[6] K. Kubota and S. Komaba, 'Review—Practical Issues and Future Perspective for Na-Ion Batteries,' *Journal of The Electrochemical Society*, vol. 162, no. 14, A2538–A2550, 2015, ISSN: 0013-4651, 1945-7111. DOI: 10.1149/2.0151514jes (cit. on p. 2).

[7] K. Nishio and N. Furukawa, 'Practical Batteries,' in *Handbook of Battery Materials, Second Edition*, Wiley-VCH Verlag GmbH & Co. KGaA, 2011, pp. 27–85, ISBN: 978-3-527-63718-8 (cit. on pp. 2, 3).

[8] D. Monti, 'Innovative electrolytes for safer sodium-ion batteries,' English, Doctoral thesis, Ph.D. dissertation, Chalmers University of Technology, 2016, ISBN: 9175973103;9789175973104; (cit. on pp. 2, 5, 16).

[9] M. Chen, J. Zhang, X. Ji, J. Fu and G. Feng, 'Progress on predicting the electrochemical stability window of electrolytes,' *Current Opinion in Electrochemistry*, vol. 34, p. 101 030, 2022, ISSN: 2451-9103. DOI: https://doi.org/10.1016/j.coelec.2022.101030 (cit. on p. 3).

[10] X. Hu, F. Feng, K. Liu, L. Zhang, J. Xie and B. Liu, 'State estimation for advanced battery management: Key challenges and future trends,' *Renewable and Sustainable Energy Reviews*, vol. 114, p. 109 334, Oct. 2019, ISSN: 1364-0321. DOI: 10.1016/j.rser.2019.109334 (cit. on p. 3).

[11] Y. Preger, H. M. Barkholtz, A. Fresquez *et al.*, 'Degradation of commercial lithium-ion cells as a function of chemistry and cycling conditions,' *Journal of The Electrochemical Society*, vol. 167, no. 12, p. 120 532, Sep. 2020. DOI: 10.1149/1945-7111/abae37 (cit. on pp. 4, 30).

[12] E. Cabrera-Castillo, F. Niedermeier and A. Jossen, 'Calculation of the state of safety (SOS) for lithium ion batteries,' *Journal of Power Sources*, vol. 324, pp. 509–520, Aug. 2016, ISSN: 0378-7753. DOI: 10.1016/j.jpowsour.2016.05.068 (cit. on p. 5).

[13] Y. Preger, L. Torres-Castro, T. Rauhala and J. Jeevarajan, 'Perspective—on the safety of aged lithium-ion batteries,' *Journal of The Electrochemical Society*, vol. 169, p. 030 507, 3 Mar. 2022, ISSN: 1945-7111. DOI: 10.1149/1945-7111/ac53cc (cit. on pp. 5, 8).

[14] P. Verma, P. Maire and P. Novák, 'A review of the features and analyses of the solid electrolyte interphase in Li-ion batteries,' English, *Electrochimica Acta*, vol. 55, no. 22, pp. 6332–6341, 2010. DOI: 10.1016/j.electacta.2010.05.072 (cit. on p. 5).

[15] G. Gachot, P. Ribière, D. Mathiron *et al.*, 'Gas chromatography/mass spectrometry as a suitable tool for the Li-ion battery electrolyte degradation mechanisms study,' English, *Analytical Chemistry*, vol. 83, no. 2, p. 478, 2011. DOI: 10.1021/ac101948u (cit. on pp. 5, 6).

[16] G. Gachot, S. Grugeon, I. Jimenez-Gordon *et al.*, 'Gas chromatography/fourier transform infrared/mass spectrometry coupling: A tool for Li-ion battery safety field investigation,' English, *Analytical Methods*, 2014. DOI: doi.org/10.1039/c4ay00054d (cit. on p. 5).

[17] G. G. Eshetu, S. Grugeon, H. Kim *et al.*, 'Comprehensive Insights into the Reactivity of Electrolytes Based on Sodium Ions,' *ChemSusChem*, vol. 9, pp. 462–471, Mar. 2016, ISSN: 18645631. DOI: 10.1002/cssc.201501605 (cit. on pp. 5, 13).

[18] R. Dugas, B. Zhang, P. Rozier and J. M. Tarascon, 'Optimization of Na-Ion Battery Systems Based on Polyanionic or Layered Positive Electrodes and Carbon Anodes,' *Journal of The Electrochemical Society*, vol. 163, no. 6, A867–A874, 2016, ISSN: 0013-4651, 1945-7111. DOI: 10.1149/2.0051605jes (cit. on p. 5).

[19] Z. Seh, J. Sun, Y. Sun and Y. Cui, 'A Highly Reversible Room-Temperature Sodium Metal Anode,' *ACS Central Science*, vol. 1, no. 8, pp. 449–455, 2015, ISSN: 2374-7943, 2374-7951. DOI: 10.1021/acscentsci.5b00328 (cit. on pp. 6, 14, 28).

[20] S. Tang and H. Zhao, 'Glymes as versatile solvents for chemical reactions and processes: From the laboratory to industry,' *RSC Advances*, vol. 4, no. 22, p. 11 251, 2014, ISSN: 2046-2069. DOI: 10.1039/c3ra47191h (cit. on pp. 6, 13).

[21] *Hyundai lithium-ion battery recall information — hyundai canada (web archive source)*. [Online]. Available: https://web.archive.org/web/20230406004236/https://www.r0183info.ca/ (visited on 23/08/2024) (cit. on pp. 6, 8).

[22] *Hyundai will replace battery systems in $900m global ev recall — automotive news*, Feb. 2021. [Online]. Available: https://www.autonews.com/regulation-safety/hyundai-will-replace-battery-systems-900m-global-ev-recall (visited on 23/08/2024) (cit. on pp. 6, 8).

[23] R. Gordon and A. Smith, 'Towards more realistic li-ion battery safety tests based on li-plating as internal cell error,' *Journal of Energy Storage*, vol. 72, p. 108 200, 2023, ISSN: 2352-152X. DOI: https://doi.org/10.1016/j.est.2023.108200 (cit. on p. 6).

[24] F. von Bülow, J. Mentz and T. Meisen, 'State of health forecasting of lithium-ion batteries applicable in real-world operational conditions,' *Journal of Energy Storage*, vol. 44, p. 103 439, Dec. 2021, ISSN: 2352-152X. DOI: 10.1016/j.est.2021.103439 (cit. on pp. 7, 35, 36, 38).

[25] M. Pasta, D. Armstrong, Z. L. Brown *et al.*, '2020 roadmap on solid-state batteries,' *Journal of Physics: Energy*, vol. 2, p. 032 008, 3 Aug. 2020. DOI: 10.1088/2515-7655/ab95f4 (cit. on p. 7).

[26] M. R. Palacin, P. Johansson, R. Dominko *et al.*, 'Roadmap on multivalent batteries,' *Journal of Physics: Energy*, vol. 6, p. 031 501, 3 May 2024, ISSN: 2515-7655. DOI: 10.1088/2515-7655/ad34fc (cit. on p. 7).

[27] J. B. Robinson, K. Xi, R. V. Kumar *et al.*, '2021 roadmap on lithium sulfur batteries,' *Journal of Physics: Energy*, vol. 3, p. 031 501, 3 Mar. 2021, ISSN: 2515-7655. DOI: 10.1088/2515-7655/abdb9a (cit. on p. 7).

[28] J. Vetter, P. Novák, M. R. Wagner *et al.*, 'Ageing mechanisms in lithium-ion batteries,' *Journal of Power Sources*, vol. 147, pp. 269–281, 1-2 Sep. 2005. DOI: 10.1016/j.jpowsour.2005.01.006 (cit. on p. 7).

[29] U. Kasavajjula, C. Wang and A. J. Appleby, 'Nano- and bulk-silicon-based insertion anodes for lithium-ion secondary cells,' *Journal of Power Sources*, vol. 163, pp. 1003–1039, 2 Jan. 2007, ISSN: 0378-7753. DOI: 10.1016/j.jpowsour.2006.09.084 (cit. on p. 7).

[30] C. R. Birkl, M. R. Roberts, E. McTurk, P. G. Bruce and D. A. Howey, 'Degradation diagnostics for lithium ion cells,' *Journal of Power Sources*, vol. 341, pp. 373–386, Feb. 2017, ISSN: 03787753. DOI: 10.1016/j.jpowsour.2016.12.011 (cit. on p. 7).

[31] S. Y. Lai, K. D. Knudsen, B. T. Sejersted, A. Ulvestad, J. P. Mæhlen and A. Y. Koposov, 'Silicon nanoparticle ensembles for lithium-ion batteries elucidated by small-angle neutron scattering,' *ACS Applied Energy Materials*, vol. 2, pp. 3220–3227, 5 May 2019, ISSN: 25740962. DOI: 10.1021/acsaem.9b00071 (cit. on p. 7).

[32] M. S. Houache, C. H. Yim, Z. Karkar and Y. Abu-Lebdeh, 'On the current and future outlook of battery chemistries for electric vehicles-mini review,' *Batteries 2022, Vol. 8, Page 70*, vol. 8, p. 70, 7 Jul. 2022, ISSN: 2313-0105. DOI: 10.3390/batteries8070070 (cit. on p. 7).

[33] X. Wang, F. Fan, J. Wang *et al.*, 'High damage tolerance of electrochemically lithiated silicon,' *Nature Communications*, vol. 6, pp. 1–7, 1 Sep. 2015, ISSN: 2041-1723. DOI: 10.1038/ncomms9417 (cit. on p. 7).

[34] A. Schiele, B. Breitung, A. Mazilkin *et al.*, 'Silicon nanoparticles with a polymer-derived carbon shell for improved lithium-ion batteries: Investigation into volume expansion, gas evolution, and particle fracture,' *ACS Omega*, vol. 3, pp. 16 706–16 713, 12 Dec. 2018, ISSN: 24701343. DOI: 10.1021/acsomega.8b02541 (cit. on p. 7).

[35] W. M. Dose, J. K. Morzy, A. Mahadevegowda, C. Ducati, C. P. Grey and M. F. D. Volder, 'The influence of electrochemical cycling protocols on capacity loss in nickel-rich lithium-ion batteries,' *Journal of Materials Chemistry A*, vol. 9, pp. 23 582–23 596, 41 Oct. 2021, ISSN: 2050-7496. DOI: 10.1039/d1ta06324c (cit. on p. 7).

[36] M. Merz, B. Ying, P. Nagel, S. Schuppler and K. Kleiner, 'Reversible and irreversible redox processes in li-rich layered oxides,' *Chemistry of Materials*, vol. 33, pp. 9534–9545, 24 Dec. 2021, ISSN: 15205002. DOI: 10.1021/acs.chemmater.1c02573 (cit. on p. 7).

[37] F. Friedrich, B. Strehle, A. T. S. Freiberg *et al.*, 'Capacity fading mechanisms of NCM-811 cathodes in lithium-ion batteries studied by X-ray diffraction and other diagnostics,' *Journal of The Electrochemical Society*, vol. 166, A3760, 15 Nov. 2019, ISSN: 1945-7111. DOI: 10.1149/2.0821915jes (cit. on p. 7).

[38] Z. Ahaliabadeh, X. Kong, E. Fedorovskaya and T. Kallio, 'Extensive comparison of doping and coating strategies for Ni-rich positive electrode materials,' *Journal of Power Sources*, vol. 540, p. 231 633, Aug. 2022, ISSN: 0378-7753. DOI: 10.1016/j.jpowsour.2022.231633 (cit. on p. 7).

[39] A. Mikheenkova, O. Gustafsson, C. Misiewicz, W. R. Brant, M. Hahlin and M. J. Lacey, 'Resolving high potential structural deterioration in Ni-rich layered cathode materials for lithium-ion batteries operando,' *Journal of Energy Storage*, vol. 57, p. 106 211, Jan. 2023, ISSN: 2352-152X. DOI: 10.1016/j.est.2022.106211 (cit. on p. 7).

[40] A. Blyr, C. Sigala, G. Amatucci, D. Guyomard, Y. Chabre and J. Tarascon, 'Self-discharge of $LiMn_2O_4$/C Li-ion cells in their discharged state: Understanding by means of three-electrode measurements,' *Journal of The Electrochemical Society*, vol. 145, pp. 194–209, 1 Jan. 1998, ISSN: 0013-4651. DOI: 10.1149/1.1838235 (cit. on p. 8).

[41] F. Liu, R. Xu, Y. Wu *et al.*, 'Dynamic spatial progression of isolated lithium during battery operations,' *Nature*, vol. 600, pp. 659–663, 7890 Dec. 2021, ISSN: 1476-4687. DOI: 10.1038/s41586-021-04168-w (cit. on p. 8).

[42] I. Traskunov and A. Latz, 'Localized fluctuations of electrochemical properties in porous electrodes of lithium-ion batteries: Beyond porous electrode theory,' *Electrochimica Acta*, vol. 379, p. 138 144, May 2021, ISSN: 00134686. DOI: 10.1016/j.electacta.2021.138144 (cit. on p. 8).

[43] A. Mistry, T. Heenan, K. Smith, P. Shearing and P. P. Mukherjee, 'Asphericity can cause nonuniform lithium intercalation in battery active particles,' *ACS Energy Letters*, vol. 7, pp. 1871–1879, 5 May 2022, ISSN: 2380-8195. DOI: 10.1021/acsenergylett.2c00870 (cit. on p. 8).

[44] M. Moshkovich, Y. Gofer and D. Aurbach, 'Investigation of the electrochemical windows of aprotic alkali metal (li, na, k) salt solutions,' *Journal of The Electrochemical Society*, vol. 148, E155, 4 Apr. 2001, ISSN: 00134651. DOI: 10.1149/1.1357316 (cit. on p. 8).

[45] R. Mogensen, D. Brandell and R. Younesi, 'Solubility of the solid electrolyte interphase (SEI) in sodium ion batteries,' *ACS Energy Letters*, vol. 1, pp. 1173–1178, 6 Dec. 2016, ISSN: 23808195. DOI: 10.1021/acsenergylett.6b00491 (cit. on p. 8).

[46] *CATL unveils its latest breakthrough technology by releasing its first generation of sodium-ion batteries*, 2021. [Online]. Available: https://www.catl.com/en/news/665.html (visited on 23/08/2024) (cit. on p. 8).

[47] US Federal Aviation Administration, *Lithium battery incident chart*. [Online]. Available: https://www.faa.gov/hazmat/resources/lithium_batteries/incidents (visited on 23/08/2024) (cit. on p. 8).

[48] Y. Chen, Y. Kang, Y. Zhao *et al.*, 'A review of lithium-ion battery safety concerns: The issues, strategies, and testing standards,' *Journal of Energy Chemistry*, vol. 59, pp. 83–99, Aug. 2021, ISSN: 2095-4956. DOI: 10.1016/j.jechem.2020.10.017 (cit. on p. 8).

[49] D. Andrea, *Battery Management Systems for Large Lithium-ion Battery Packs* (EBL-Schweitzer). Artech House, 2010, ISBN: 9781608071050 (cit. on pp. 9, 10).

[50] A. Rasheed, O. San and T. Kvamsdal, 'Digital twin: Values, challenges and enablers from a modeling perspective,' *IEEE Access*, vol. 8, pp. 21 980–22 012, 2020, ISSN: 21693536. DOI: 10.1109/access.2020.2970143 (cit. on p. 10).

[51] A. Sancarlos, M. Cameron, A. Abel, E. Cueto, J. L. Duval and F. Chinesta, 'From ROM of electrochemistry to AI-based battery digital and hybrid twin,' *Archives of Computational Methods in Engineering*, vol. 28, pp. 979–1015, May 2021, ISSN: 18861784. DOI: 10.1007/s11831-020-09404-6 (cit. on p. 10).

[52] B. Wu, W. D. Widanage, S. Yang and X. Liu, 'Battery digital twins: Perspectives on the fusion of models, data and artificial intelligence for smart battery management systems,' *Energy and AI*, vol. 1, p. 100 016, Aug. 2020, ISSN: 26665468. DOI: 10.1016/j.egyai.2020.100016 (cit. on pp. 10, 11).

[53] W. Li, M. Rentemeister, J. Badeda, D. Jöst, D. Schulte and D. U. Sauer, 'Digital twin for battery systems: Cloud battery management system with online state-of-charge and state-of-health estimation,' *Journal of Energy Storage*, vol. 30, p. 101 557, Aug. 2020, ISSN: 2352-152X. DOI: 10.1016/j.est.2020.101557 (cit. on p. 11).

[54] P. M. Attia, A. Grover, N. Jin *et al.*, 'Closed-loop optimization of fast-charging protocols for batteries with machine learning,' *Nature*, vol. 578, pp. 397–402, 7795 Feb. 2020, ISSN: 1476-4687. DOI: 10.1038/s41586-020-1994-5 (cit. on pp. 11, 45).

[55] J. M. Reniers, G. Mulder and D. A. Howey, 'Unlocking extra value from grid batteries using advanced models,' *Journal of Power Sources*, vol. 487, p. 229 355, Mar. 2021, ISSN: 03787753. DOI: 10.1016/j.jpowsour.2020.229355 (cit. on p. 11).

[56] M. Baumann, S. Rohr and M. Lienkamp, 'Cloud-connected battery management for decision making on second-life of electric vehicle batteries,' *2018 13th International Conference on Ecological Vehicles and Renewable Energies, EVER 2018*, pp. 1–6, May 2018. DOI: 10.1109/ever.2018.8362355 (cit. on p. 11).

[57] D. Beverungen, B. Klör, S. Bräuer and M. Monhof, 'Will they die another day? a decision support perspective on reusing electric vehicle batteries,' *ECIS 2015 Research-in-Progress Papers*, May 2015 (cit. on p. 11).

[58] A. Ponrouch, A. Goñi and M. R. Palacín, 'High capacity hard carbon anodes for sodium ion batteries in additive free electrolyte,' *Electrochemistry Communications*, vol. 27, pp. 85–88, 2013, ISSN: 13882481. DOI: 10.1016/j.elecom.2012.10.038 (cit. on p. 13).

[59] D. A. Stevens and J. R. Dahn, 'High Capacity Anode Materials for Rechargeable Sodium-Ion Batteries,' *Journal of The Electrochemical Society*, vol. 147, no. 4, pp. 1271–1273, 2000. DOI: 10.1149/1.1393348 (cit. on pp. 13, 30).

[60] Y.-U. Park, D.-H. Seo, H. Kim *et al.*, 'A Family of High-Performance Cathode Materials for Na-ion Batteries, $Na_3(VO_{1-x}PO_4)_2F_{1+2x}$ $(0 < x < 1)$: Combined First-Principles and Experimental Study,' *Advanced Functional Materials*, vol. 24, no. 29, pp. 4603–4614, 2014, ISSN: 1616301X. DOI: 10.1002/adfm.201400561 (cit. on p. 13).

[61] B. Zhang, R. Dugas, G. Rousse, P. Rozier, A. M. Abakumov and J.-M. Tarascon, 'Insertion compounds and composites made by ball milling for advanced sodium-ion batteries,' *Nature Communications*, vol. 7, p. 10 308, 2016, ISSN: 2041-1723. DOI: 10.1038/ncomms10308 (cit. on p. 13).

[62] D. Aurbach, M. Daroux, P. Faguy and E. Yeager, 'The electrochemistry of noble metal electrodes in aprotic organic solvents containing lithium salts,' *Journal of Electroanalytical Chemistry and Interfacial Electrochemistry*, vol. 297, pp. 225–244, 1 Jan. 1991, ISSN: 0022-0728. DOI: 10.1016/0022-0728(91)85370-5 (cit. on pp. 14, 28).

[63] M. Yudanov, C. Palm, L. Ögren and K. Westman, *Catalysts for a more efficient splitting of water*, Chalmer University of Technology, Bachelor Thesis, 2014 (cit. on p. 15).

[64] I. C. Man, H.-Y. Su, F. Calle-Vallejo *et al.*, 'Universality in oxygen evolution electrocatalysis on oxide surfaces,' *ChemCatChem*, vol. 3, no. 7, pp. 1159–1165, 2011, ISSN: 1867-3899. DOI: 10.1002/cctc.201000397 (cit. on p. 16).

[65] A. C. Lazanas and M. I. Prodromidis, 'Electrochemical impedance spectroscopy–a tutorial,' *ACS Measurement Science Au*, vol. 3, pp. 162–193, 3 Jun. 2023, ISSN: 2694250X. DOI: 10.1021/acsmeasuresciau.2c00070 (cit. on p. 16).

[66] E. Barsoukov and J. R. Macdonald, Eds., *Impedance spectroscopy: theory, experiment, and applications*, 2. ed. Wiley-Interscience, 2005, ISBN: 978-0-471-64749-2 (cit. on p. 17).

[67] P. K. Jones, U. Stimming and A. A. Lee, 'Impedance-based forecasting of lithium-ion battery performance amid uneven usage,' *Nature Communications*, vol. 13, pp. 1–9, 1 Aug. 2022, ISSN: 2041-1723. DOI: 10.1038/s41467-022-32422-w (cit. on p. 17).

[68] *Fourier transform infrared spectroscopy*, 2016. [Online]. Available: https://en.wikipedia.org/wiki/Fourier-transform_infrared_spectroscopy (visited on 23/08/2024) (cit. on p. 17).

[69] M. Libarondi and J. Binkley, 'Comparing the Capabilities of Time-of-Flight and Quadrupole Mass Spectrometers,' *LCGC Supplements*, vol. 8, 3 2010 (cit. on p. 18).

[70] Linde Group, *Gas chromatography*. [Online]. Available: https://hiq.linde-gas.com/en/analytical_methods/gas_chromatography/index.html (visited on 23/08/2024) (cit. on p. 18).

[71] M. D. Wilkinson, M. Dumontier, I. J. Aalbersberg *et al.*, 'The fair guiding principles for scientific data management and stewardship,' *Scientific Data 2016 3:1*, vol. 3, pp. 1–9, 1 Mar. 2016, ISSN: 2052-4463. DOI: 10.1038/sdata.2016.18 (cit. on pp. 22, 23).

[72] J. Pearl, *Causality - Models Reasoning and Inference*, 2nd ed. Cambridge University Press, 2009 (cit. on pp. 24, 25).

[73] A. Molak, *Causal Inference and Discovery in Python: Unlock the Secrets of Modern Causal Machine Learning with DoWhy, EconML, PyTorch and More*. Packt Publishing, Limited, 2023, ISBN: 9781804612989 (cit. on p. 24).

[74] K. Saravanan, C. W. Mason, A. Rudola, K. H. Wong and P. Balaya, 'The First Report on Excellent Cycling Stability and Superior Rate Capability of Na $_3$ V $_2$ (PO $_4$) $_3$ for Sodium Ion Batteries,' *Advanced Energy Materials*, vol. 3, no. 4, pp. 444–450, 2013, ISSN: 16146832. DOI: 10.1002/aenm.201200803 (cit. on p. 27).

[75] V. Palomares, P. Serras, I. Villaluenga, K. B. Hueso, J. Carretero-González and T. Rojo, 'Na-ion batteries, recent advances and present challenges to become low cost energy storage systems,' *Energy & Environmental Science*, vol. 5, pp. 5884–5901, 3 2012. DOI: 10.1039/c2ee02781j (cit. on p. 27).

[76] A. Ponrouch, D. Monti, A. Boschin, B. Steen, P. Johansson and M. R. Palacín, 'Non-aqueous electrolytes for sodium-ion batteries,' *Journal of Materials Chemistry A*, vol. 3, no. 1, pp. 22–42, 2015. DOI: 10.1039/c4ta04428b (cit. on p. 30).

[77] Wikipedia, *Vanadium compounds - wikipedia*. [Online]. Available: https://en.wikipedia.org/wiki/Vanadium_compounds (visited on 22/08/2024) (cit. on p. 33).

[78] V. Sulzer, P. Mohtat, A. Aitio *et al.*, 'The challenge and opportunity of battery lifetime prediction from field data,' *Joule*, vol. 5, pp. 1934–1955, 8 Aug. 2021, ISSN: 2542-4351. DOI: 10.1016/j.joule.2021.06.005 (cit. on p. 34).

[79] G. Samuel and D. Howey, 'Automated feature extaction and selection for data-driven models of rapid battery capacity fade and end of life,' *IEEE Transactions on Industrial Informatics*, 2021, ISSN: 19410050. DOI: 10.1109/tii.2021.3106593 (cit. on pp. 34, 35, 38).

[80] M. Attia Peter, B. Alexander, B. Planella Ferran *et al.*, 'Review—"knees" in lithium-ion battery aging trajectories,' *Journal of The Electrochemical Society*, vol. 169, 6 2022. DOI: 10.1149/1945-7111/ac6d13 (cit. on p. 34).

[81] Y. Zhang, T. Wik, J. Bergström, M. Pecht and C. Zou, 'A machine learning-based framework for online prediction of battery ageing trajectory and lifetime using histogram data,' *Journal of Power Sources*, vol. 526, p. 231 110, Apr. 2022, ISSN: 0378-7753. DOI: 10.1016/j.jpowsour.2022.231110 (cit. on pp. 34, 35, 38, 39).

[82] R. R. Richardson, M. A. Osborne and D. A. Howey, 'Gaussian process regression for forecasting battery state of health,' *Journal of Power Sources*, vol. 357, pp. 209–219, Jul. 2017, ISSN: 0378-7753. DOI: 10.1016/j.jpowsour.2017.05.004 (cit. on pp. 34, 35).

[83] V. Sulzer, P. Mohtat, S. Lee, J. B. Siegel and A. G. Stefanopoulou, 'Promise and challenges of a data-driven approach for battery lifetime prognostics,' *Proceedings of the American Control Conference*, vol. 2021-May, pp. 4427–4433, May 2021, ISSN: 07431619. DOI: 10.23919/acc50511.2021.9483312 (cit. on p. 34).

[84] W. Li, H. Zhang, B. van Vlijmen, P. Dechent and D. U. Sauer, 'Forecasting battery capacity and power degradation with multi-task learning,' *Energy Storage Materials*, vol. 53, pp. 453–466, Dec. 2022, ISSN: 2405-8297. DOI: 10.1016/j.ensm.2022.09.013 (cit. on pp. 34, 35).

[85] A. Aitio and D. A. Howey, 'Predicting battery end of life from solar off-grid system field data using machine learning,' *Joule*, Jul. 2021, ISSN: 25424351. DOI: 10.1016/j.joule.2021.11.006 (cit. on p. 34).

[86] R. Ibraheem, C. Strange and G. dos Reis, 'Capacity and internal resistance of lithium-ion batteries: Full degradation curve prediction from voltage response at constant current at discharge,' *Journal of Power Sources*, vol. 556, p. 232 477, Feb. 2023, ISSN: 0378-7753. DOI: 10.1016/j.jpowsour.2022.232477 (cit. on p. 34).

[87] K. A. Severson, P. M. Attia, N. Jin *et al.*, 'Data-driven prediction of battery cycle life before capacity degradation,' *Nature Energy*, vol. 4, pp. 383–391, 5 Mar. 2019, ISSN: 2058-7546. DOI: 10.1038/s41560-019-0356-8 (cit. on pp. 35, 39).

[88] H. Johnsson, 'A neural network approach to absolute state-of-health estimation in electric vehicles battery degradation study based on fleet data,' M.S. thesis, Chalmers University of Technology, 2018 (cit. on p. 35).

[89] S. Greenbank and D. A. Howey, 'Piecewise-linear modelling with automated feature selection for Li-ion battery end-of-life prognosis,' *Mechanical Systems and Signal Processing*, vol. 184, p. 109 612, Feb. 2023, ISSN: 0888-3270. DOI: 10.1016/j.ymssp.2022.109612 (cit. on pp. 35, 38).

[90] A. Nuhic, T. Terzimehic, T. Soczka-Guth, M. Buchholz and K. Dietmayer, 'Health diagnosis and remaining useful life prognostics of lithium-ion batteries using data-driven methods,' *Journal of Power Sources*, vol. 239, pp. 680–688, Oct. 2013, ISSN: 0378-7753. DOI: 10.1016/j.jpowsour.2012.11.146 (cit. on pp. 35, 38).

[91] R. R. Richardson, C. R. Birkl, M. A. Osborne and D. A. Howey, 'Gaussian process regression for in situ capacity estimation of lithium-ion batteries,' *IEEE Transactions on Industrial Informatics*, vol. 15, pp. 127–138, 1 Jan. 2019, ISSN: 15513203. DOI: 10.1109/tii.2018.2794997 (cit. on p. 35).

[92] C. Gervillié-Mouravieff, C. Boussard-Plédel, J. Huang *et al.*, 'Unlocking cell chemistry evolution with operando fibre optic infrared spectroscopy in commercial Na(Li)-ion batteries,' *Nature Energy 2022 7:12*, vol. 7, pp. 1157–1169, 12 Nov. 2022, ISSN: 2058-7546. DOI: 10.1038/s41560-022-01141-3 (cit. on p. 36).

[93] D. Liu, J. Pang, J. Zhou, Y. Peng and M. Pecht, 'Prognostics for state of health estimation of lithium-ion batteries based on combination gaussian process functional regression,' *Microelectronics Reliability*, vol. 53, pp. 832–839, 6 Jun. 2013, ISSN: 0026-2714. DOI: 10.1016/j.microrel.2013.03.010 (cit. on p. 38).

[94] I. Buchberger, S. Seidlmayer, A. Pokharel *et al.*, 'Aging analysis of graphite/$LiNi_{1/3}$ $Mn_{1/3}$ $Co_{1/3}$ O_2 cells using XRD, PGAA, and AC impedance,' *Journal of The Electrochemical Society*, vol. 162, A2737–A2746, 14 Oct. 2015, ISSN: 0013-4651. DOI: 10.1149/2.0721514jes (cit. on p. 42).

[95] R. Jung, F. Linsenmann, R. Thomas *et al.*, 'Nickel, manganese, and cobalt dissolution from ni-rich nmc and their effects on NMC622-graphite cells,' *Journal of The Electrochemical Society*, vol. 166, A378–A389, 2 Feb. 2019, ISSN: 0013-4651. DOI: 10.1149/2.1151902jes (cit. on p. 42).

[96] P. Desai, J. Huang, D. Foix, J.-M. Tarascon and S. Mariyappan, 'Zero volt storage of na-ion batteries: Performance dependence on cell chemistry!' *Journal of Power Sources*, vol. 551, p. 232 177, 2022, ISSN: 0378-7753. DOI: 10.1016/j.jpowsour.2022.232177 (cit. on p. 42).

[97] A. Ponrouch, R. Dedryvère, D. Monti *et al.*, 'Towards high energy density sodium ion batteries through electrolyte optimization,' *Energy & Environmental Science*, vol. 6, no. 8, p. 2361, 2013. DOI: 10.1039/c3ee41379a (cit. on p. 44).

[98] J. Groot, 'State-of-health estimation of li-ion batteries: Ageing models,' Ph.D. dissertation, Chalmer University of Technology, 2014, ISBN: 9789175971346 (cit. on p. 45).